

Peak Effect in $\text{Ca}_3\text{Rh}_4\text{Sn}_{13}$: Vortex Phase Diagram and Evidences for Stepwise Amorphization of Flux Line Lattice

S. Sarkar^{1*}, D. Pal¹, S. S. Banerjee¹, S. Ramakrishnan¹, A. K. Grover^{1†}, C. V. Tomy²,
G. Ravikumar³, P. K. Mishra³, V. C. Sahni³, G. Balakrishnan⁴, D. McK. Paul⁴ and
S. Bhattacharya^{1,5}

¹*Department of Condensed Matter Physics and Materials Science,*

Tata Institute of Fundamental Research, Colaba, Mumbai 400005, India

²*Department of Physics, Indian Institute of Technology, Powai, Mumbai 400076, India*

³*Technical Physics and Prototype Engineering Division, Bhabha Atomic Research Centre,
Mumbai 400 085, India*

⁴*Department of Physics, University of Warwick, Coventry CV4 7AL, U.K.*

⁵*NEC Research Institute, 4 Independence Way, Princeton, N. J. 08540*

Abstract

The Peak Effect (PE) regime in a single crystal of $\text{Ca}_3\text{Rh}_4\text{Sn}_{13}$ has been investigated in detail via ac susceptibility as well as dc magnetization measurements. The PE region comprises two discontinuous first order like transitions, located near its *onset* and *peak* positions and reflects a stepwise fracturing of the flux line lattice (FLL). This scenario can be construed as an alternative to a scheme involving the appearance of Generalized Fulde-Ferrel-Larkin-Ovchinnikov (GFFLO) state as considered in the case of PE phenomenon in isostructural $\text{Yb}_3\text{Rh}_4\text{Sn}_{13}$ system. The procedure of thermal cycling across

*E-mail:shampa@tifr.res.in

†E-mail:grover@tifr.res.in

the onset position of PE produces an open hysteresis loop, which is consistent with the notion of the fracturing of the FLL. A study of thermomagnetic history dependence of different metastable vortex states shows the path dependence in the critical current density $J_c(H, T)$ over a large part of the (H, T) parameter space. The path dependence in J_c ceases above the *peak* position of the PE, suggesting a complete amorphization and the loss of long range correlations of the FLL at (T_p, H_p) line. A plausible vortex phase diagram has been illustrated for $\text{Ca}_3\text{Rh}_4\text{Sn}_{13}$ and phases like an elastic solid, a plastic solid, a pinned amorphous and an unpinned amorphous states have been identified.

PACS code: 64.70 Dv, 74.60 Ge, 74.25 Dw, 74.60 Ec, 74.60 Jg

Keywords : Peak Effect, order to disorder transformation, vortex phase diagram, $\text{Ca}_3\text{Rh}_4\text{Sn}_{13}$

I. INTRODUCTION

Peak Effect (PE) phenomenon relates to an anomalous behavior of (macroscopic) current carrying capacity in the mixed state of a type II superconductor. The critical current density J_c of a superconductor, which usually decreases monotonically with increasing H or T , can show an anomalous increase before proceeding to zero at or close to the superconducting to normal phase boundary ($H_{c2}/T_c(H)$ line). The occurrence of PE, ubiquitous in conventional low temperature superconductors, has received a considerable amount of attention in recent years [1–14]. A large variety of superconducting systems exhibit PE, such as, Nb (pure metal) [7], V_3Si (*A15* compound) [8], $2H-NbSe_2$ (layered chalcogenide) [1,10,11], rare earth intermetallics, like, $CeCo_2$ [9] and $CeRu_2$ [2,5,6], $Yb_3Rh_4Sn_{13}$ (ternary stannide) [12,13], YNi_2B_2C (quarternary borocarbide) [14], UPd_2Al_3 (heavy fermion superconductor) [3,4], $YBa_2Cu_3O_7$ (high temperature superconductor) [15,16], etc. Of the various scenarios being considered to understand PE phenomenon, two appear distinct and independent. A classical scenario, originally due to Pippard [17], attempts to relate PE to a faster rate of decrease in elastic moduli of FLL with increase in temperature as compared to that of the elementary pinning force. A recent scenario due to Tachiki et al [4], suggests that PE phenomenon in heavy fermion superconductors (HFS) could be caused as a first order transition by the realization of a generalized Fulde-Ferrel-Larkin-Ovchinnikov (GFFLO) [18,19] state at high fields and low temperatures ($T \leq 0.55T_c(0)$). The rare earth and Uranium based superconductors have large normal state paramagnetism, and in the superconducting mixed state of these systems, the order parameter can assume a spatial modulation (with nodes in the longitudinal direction) at high fields such that the vortex line (then) comprises coupled segments of lengths comparable to wavelength of modulation in superconducting order parameter. The inevitably present pinning centres in the sample enhance their pinning action on such vortex lines at the onset of GFFLO transition and thereby cause PE phenomenon.

Modler et al [3] have shown that the characteristics of several physical properties in the

PE region of a single crystal of the heavy fermion compound UPd_2Al_3 are similar to those in a single crystal of the mixed valent compound CeRu_2 and the phase boundaries (locus of H and T values) drawn for UPd_2Al_3 and CeRu_2 extend over similar parametric limits in the (H, T) space [20]. Sato et al [12], followed by Tomy et al [13], reported observation of the PE and the construction of a magnetic phase diagram in weakly pinned crystals of $\text{Yb}_3\text{Rh}_4\text{Sn}_{13}$, which bore striking resemblance to such phase diagrams in UPd_2Al_3 and CeRu_2 [3]. On the other hand, Crabtree et al [21] have drawn attention to the similarities in the details of the transport studies on the PE phenomenon in single crystals of CeRu_2 and $\text{YBa}_2\text{Cu}_3\text{O}_7$ with those observed in crystals of $2H\text{-NbSe}_2$ [1]. The latter system, $2H\text{-NbSe}_2$, is thought to be an archetypal example for the classical scenario of collapse of elastic moduli of flux line lattice (FLL) (implying a thermal and/or disorder induced amorphization of the FLL [1,22]) as a source of PE. Very recently, Banerjee et al [23] have shown that in crystals of $2H\text{-NbSe}_2$ and CeRu_2 , having comparable levels of pinning, the PE phenomenon comprises a rich structure that can be construed as an evidence of a stepwise fracturing of the vortex lattice at or near the incipient FLL melting transition in both the systems. It is asserted [23] that the destruction of the elastically deformed vortex solid commences at the onset of PE via a pinning-induced fracturing transition and the amorphization of the vortex solid proceeds to completion at the peak position of PE due to juxtaposition of effects caused by thermal fluctuations and quenched random disorder. Between the onset and the peak positions of the PE, the vortex solid is believed to be in a plastically deformed state, as revealed by earlier transport studies in $2H\text{-NbSe}_2$ [1] and CeRu_2 [21].

Independent of these developments, Tomy et al [24] have reported the occurrence of PE and the construction of a magnetic phase diagram in $\text{Ca}_3\text{Rh}_4\text{Sn}_{13}$, which again bear striking resemblance to those in UPd_2Al_3 and CeRu_2 [3]. This ternary system has the same crystal structure as the ternary rare earth stannide $\text{Yb}_3\text{Rh}_4\text{Sn}_{13}$ [12,13], but, it does not contain any rare earth ions. Its normal state paramagnetic value of 3.3×10^{-6} emu/cm³ precludes the realization of a GFFLO state [4] in it. In view of an apparent similarity in the magnetic phase

diagram of $\text{Ca}_3\text{Rh}_4\text{Sn}_{13}$ with those in other compounds like $\text{Yb}_3\text{Rh}_4\text{Sn}_{13}$, $2H\text{-NbSe}_2$, CeRu_2 , CeCo_2 , UPd_2Al_3 , etc., it is of interest to investigate the detailed behaviour in the PE region of $\text{Ca}_3\text{Rh}_4\text{Sn}_{13}$, and to compare them with the results of Banerjee et al [23] and Ravikumar et al [25] in $2H\text{-NbSe}_2$ and CeRu_2 . We report here the results of an extensive investigation of the PE phenomenon in a single crystal sample of $\text{Ca}_3\text{Rh}_4\text{Sn}_{13}$ through temperature and magnetic field dependence of ac susceptibility and dc magnetization measurements. Our results indeed reveal the existence of a characteristic structure, nearly identical to that observed earlier in CeRu_2 and $2H\text{-NbSe}_2$ [23]. The PE region in $\text{Ca}_3\text{Rh}_4\text{Sn}_{13}$ spans two sharp transitions located at its *onset* and *peak* positions and a characteristic hysteretic effect is observed on thermal cycling across the transition located at the onset. Prior to the peak position of the PE, the state of the vortex array and its current carrying capacity J_c depends on its thermomagnetic history, i.e., J_c in the vortex array created in the field cooled (FC) manner is much larger than that in the zero field cooled (ZFC) manner [25,26]. The isothermal dc magnetization hysteresis experiments also reveal a characteristic path dependence in J_c . The new results being reported here, therefore, support the generic nature of process of disordering of FLL under the combined influence of quenched random disorder (pinning) and thermal fluctuations.

II. EXPERIMENTAL DETAILS

The single crystal of $\text{Ca}_3\text{Rh}_4\text{Sn}_{13}$ ($3.4 \times 3.2 \times 0.6 \text{ mm}^3$, 48.1 mg) used in the present studies is from the same batch, grown by the tin flux method and utilized by Tomy et al [24]. The $T_c(0)$ of $\text{Ca}_3\text{Rh}_4\text{Sn}_{13}$ is 8.18 K and it crystallizes in the Phase-1 structure (primitive cubic). The ac susceptibility measurements in superposed dc magnetic fields have been performed using a well-shielded home built ac susceptometer [27]. The ac and dc fields are co-axial and the sample is placed in such a way that one of its principal axis (cube edge) is always aligned parallel with the field (i.e., $H // [001]$). The ac measurements were usually made at a frequency of 211 Hz and with an ac amplitude of 1 Oe (r.m.s.). The dc magnetization

data were obtained on a commercial SQUID magnetometer (Quantum Design Inc., U.S.A, Model MPMS 5), but using a new procedure designated as *Half Scan Technique* (HST) by Ravikumar et al [28]. The magnetization values obtained via HST minimize the artifacts arising due to the sample movement through the inhomogeneous magnetic field in the SQUID magnetometer and are independent of the choice of the scan length. Tomy et al [24] had earlier obtained dc magnetization values in their crystal of $\text{Ca}_3\text{Rh}_4\text{Sn}_{13}$ with (full) scan length of 2 cm and using the usual full scan (FS) analysis procedure as prescribed by the MPMS software. Ravikumar et al [28] have focussed attention on to the differences in the magnetization values in the PE region of CeRu_2 and $2H\text{-NbSe}_2$ obtained by HST and FS analysis. We have noted similar differences for $\text{Ca}_3\text{Rh}_4\text{Sn}_{13}$ crystal as well and have, therefore, used the HST procedure to acquire the dc magnetization data reported here.

III. EXPERIMENTAL RESULTS

A. MANIFESTATION OF PEAK EFFECT VIA ISOFIELD AC SUSCEPTIBILITY AND ISOTHERMAL DC MAGNETIZATION MEASUREMENTS

I. ISOFIELD AC SUSCEPTIBILITY MEASUREMENTS

Figures 1(a), 1(b), and 1(c) show the temperature dependence of the real part of the ac susceptibility ($\chi'(T)$) for a $\text{Ca}_3\text{Rh}_4\text{Sn}_{13}$ crystal in various dc bias fields maintained parallel to the [001] plane of the crystal. The FLL was prepared in the zero field cooled (ZFC) mode (i.e., the superconducting sample was initially cooled to the lowest temperature in zero magnetic field and subsequently a given value of the dc field was applied). The screening response was then measured while warming up the sample. Figure 1(a) shows the typical variation of $\chi'(T)$ in low applied fields (0 - 2.5 kOe). In zero field, $\chi'(T)$ response shows perfect screening ($\chi' \approx -1$) at low temperatures and a sharp transition towards normal state near the superconducting transition temperature $T_c(0)$. As the applied field increases, the superconducting to normal transition broadens and $\chi'(T)$ rises monotonically to its normal

state value at $T_c(H)$. However, for an applied dc field of 3.5 kOe, as shown in the top panel of Fig. 1(b), this monotonic behaviour is interrupted by an anomalous dip in $\chi'(T)$ at a temperature denoted as $T = T_p$ (= 7.43 K at 3.5 kOe).

Within the Bean's critical state model (CSM) [29,15], $\chi'(T)$ can be approximated as,

$$\chi'(T) \sim -1 + (\alpha h_{ac}/J_c), \quad (1)$$

where α is a geometry dependent factor, h_{ac} is the applied ac field and J_c is the critical current density. The above relation implies that the dip in $\chi'(T)$ is a consequence of enhancement in J_c , the ubiquitous Peak Effect. As the dc bias field is increased further (e.g. to $H_{dc} = 5$ kOe), the tiny dip in the top panel of Fig. 1(b) transforms to a double peak structure, as shown in the bottom panel of Fig. 1(b). This two-dip structure becomes progressively more prominent as the dc field increases and the peak effect phenomenon eventually comprises two very sharp (≤ 5 mK width) first order like transitions as implied by the data in Fig. 1(c). For instance, in a field of 10 kOe in Fig. 1(c), $\chi'(T)$ displays a sharp (≤ 5 mK) dip at $T = T_{pl}$ (the so called *onset* temperature of the peak effect), followed by another sharp dip at $T = T_p$ (the *peak* temperature). Above T_p , the $\chi'(T)$ response shows a rapid recovery towards the zero value. The occurrence of sharp changes in J_c at the *onset* and the *peak* positions of the PE were not apparent in isothermal $\chi'(H)$ scans performed earlier by Tomy et al [24] in the same crystal. However, the $T_p(H)$ values observed in the present isofield measurements show good agreement with $H_p(T)$ values reported by Tomy et al [24]. It is interesting to note how rapidly the PE regime evolves with increasing field. A more than ten-fold increase can be noted in the extent of the anomalous dip in $\chi'(T)$ values characterising the PE between $H_{dc} = 3.5$ kOe and 5 kOe. Also, the recovery of $\chi'(T)$ above T_p to its normal state value becomes steeper as the field increases (cf. plots in Figs.1(b) and 1(c)), thus indicating the sharpness of the transformation in the state of vortex matter occurring across the peak position of the PE.

The inset of Fig. 1(c) summarizes T_{pl} and T_p values, plotted in the (H, T) phase diagram, for various dc bias fields. Below 5 kOe, one can hardly distinguish between T_{pl} and T_p values

of the PE, and T_{pl} and T_p curves appear to merge at a multicritical point corresponding to $T_p(H)/T_c(0) \sim 0.9$ in the phase diagram. The lowest field down to which a residual signature of a peak could be ascertained in our data is 3.5 kOe which corresponds to a $T_p(H)/T_c(0)$ value of about 0.91.

II. ISOTHERMAL DC MAGNETIZATION RESULTS

In order to further explore the different facets of PE observed in the ac susceptibility measurements, isothermal dc magnetization hysteresis measurements were also performed on the same crystal. The results at two temperatures are shown in Fig. 2. Magnetization curves were recorded for increasing as well as decreasing field cycles over a total scan length of 4 cm using the new HST as well as the conventional FS method on a SQUID magnetometer. The magnetization data recorded at 4.5 K shows a clear hysteresis in the field interval 15 -19 kOe between the forward($H \uparrow$) and the reverse($H \downarrow$) legs of the field sweep. According to the Bean's critical state model (CSM) [29], this hysteresis in magnetization $\Delta M(H) = M(H \uparrow) - M(H \downarrow)$ provides a measure of the macroscopic critical current density $J_c(H)$ and is a distinct indicator of the occurrence of the PE. The field where the magnetization hysteresis bubble is widest identifies the peak field H_p and the collapse of hysteresis locates the irreversibility field H_{irr} , above which the critical current density falls below the measurable limit of the method used (see Fig. 2).

In the main panel of Fig. 2 at 4.5 K, it is apparent that the hysteresis width in the peak effect region measured by the HST is significantly larger (and the hysteresis bubble is much more symmetric) than that measured using the conventional FS procedure. It is also to be noted that the use of HST results in measurable values of magnetization hysteresis below the onset of the PE, whereas the FS method results in the near absence of magnetization hysteresis in the same field region. The observed distinction is important in the sense that the isofield ac susceptibility measurements show diamagnetic $\chi'(T)$ response (see Figs 1(a) to 1(c)) prior to the arrival of PE regime, which clearly demands that the dc magnetization should not be reversible prior to PE (i.e., $J_c \neq 0$). These results demonstrate the efficacy and the necessity of the HST employed in our isothermal dc magnetization measurements. To

illustrate the point even further, the two insets of Fig. 2 show a comparison of magnetization hysteresis data obtained by HST and FS method at 6.1 K, where the peak field is expected to be about 10 kOe (cf. Fig. 1(c)). A clear signature of the PE can be observed in dc magnetization measurements only if the *half scan technique* is used.

Even while the PE hysteretic bubble recorded with HST at 4.5 K is more symmetric than that recorded with FS method, and undoubtedly the proper technique to utilise, nevertheless the difference in fields marking the onset and offset of PE in the forward and reverse legs of the bubble persists, i.e., $H_{pl}^f > H_{pl}^r$, i.e., this feature is not an artifact of the method used but is a characteristic property of the system. Such differences in the *onset* (H_{pl}^f) and the *offset* (H_{pl}^r) fields of the PE have been widely noticed in several low T_c and high T_c systems, like, UPd₂Al₃ [3], CeRu₂ [2], 2H-NbSe₂ [23], Yb₃Rh₄Sn₁₃ [12,13], YBa₂Cu₃O₇ [30], etc., and have led to the proposition that the onset of the PE is akin to a first order phase transition [2,3,6,28,30]. A first order change allows for the possibility of the existence of thermal hysteresis and the path dependence in the values of some physical variables, which in our case is the current density J_c .

B. THE DISORDER AND THE HISTORY DEPENDENCE OF THE MACROSCOPIC CRITICAL CURRENT DENSITY J_c

I. ISOFIELD AC SUSCEPTIBILITY STUDY:

We have explored the thermomagnetic history effects in J_c in the PE region through the temperature dependent ac susceptibility measurements. Two different sample histories, viz., the ZFC and the FC, commonly associated with disordered magnets such as spin glasses, were investigated. In the FC mode, the sample was rapidly cooled down from the normal state in the presence of an applied dc field and then the measurements were performed while warming up the FLL (i.e., the field-cooled warm up (FCW) mode). Figure 3 displays the typical response of $\chi'(T)$ for two thermomagnetic histories in a field of 10 kOe in Ca₃Rh₄Sn₁₃. The FLL states in the FCW mode can be seen to give larger diamagnetic screening response

as compared to those produced via ZFC mode over a wide range of temperature, up to the peak position of the PE.

Since the macroscopic current density J_c is directly related to the $\chi'(T)$ response (Eq.1), the differences in $\chi'(T)$ responses between the ZFC and FCW modes reveal the history dependence of the macroscopic critical current density J_c in those modes, i.e., $J_c^{FCW}(T) > J_c^{ZFC}(T)$ for $T < T_p$. In an earlier report, Banerjee et al [23] have exhibited the same kind of history dependence in single crystals of CeRu₂ and 2H-NbSe₂. Also, from a small angle neutron scattering study, Huxley et al [31] have surmised that the FC state in CeRu₂ comprises more finely divided regions of correlated lattice as compared to those in the ZFC state. The difference in ZFC and FCW responses was finally found to disappear at the peak position of the PE, somewhat akin to the magnetic responses in spin glasses where the ZFC and FC magnetization curves merge at the spin glass transition temperature T_g [32]. Unlike the spin glasses, where the glass temperature T_g could display measurable differences on variation of the frequency and the amplitude of the ac field, at least in the vortex system in Ca₃Rh₄Sn₁₃ (see Fig. 4), the onset (T_{pl}) and the peak (T_p) temperatures of PE do not vary with the change in frequency and/or amplitude of the ac field. Figures 4(a) and 4(b) display the $\chi'(T)$ response in ZFC mode at 10 kOe, when frequency is changed from 211 Hz to 21 Hz (ac amplitude is kept constant) and the ac amplitude is changed from 1 Oe to 3.5 Oe (r.m.s) (ac frequency is kept constant). The observed robust independence of T_{pl} and T_p on the amplitude and especially on the frequency, further attests to the first order nature of the transformations and the consequent absence of pretransitional fluctuation effects, such as, critical slowing down, etc..

II. ISOTHERMAL DC MAGNETIZATION DATA:

To further elucidate the thermomagnetic history effects in $J_c(H, T)$ in Ca₃Rh₄Sn₁₃, Fig. 5 summarises the magnetization hysteresis curves recorded after obtaining the vortex states in FC mode at fields lying well below as well as within the PE region at $T = 4.5$ K. As per CSM description of magnetization hysteresis data [33], when the critical current den-

sity is uniquely prescribed for a vortex state at a given H and T , the single-valuedness of $J_c(H)$ demands that all the magnetization values obtained along various paths with different thermomagnetic histories should lie within the envelope loop defined by the forward and the reverse branches of the magnetization curve obtained in isothermal dc magnetization measurements [33,34]. The dc magnetization data illustrated in Fig.5 go beyond the above description and elucidate the multi-valued nature of $J_c(H)$. Figure 5 shows that as the sample is cooled in a pre-selected magnetic field ($H_i < H_p$) to the required temperature (FC mode) and the magnetization is recorded as a function of increasing/decreasing fields, the initial magnetization values (respectively) *overshoot* the forward/reverse magnetization envelope curves. On further increasing/decreasing the field, the magnetization values fall sharply and merge into the usual envelope loop (to be identified by the thin continuous lines in Fig. 5). The *overshooting* by the initial magnetization values clearly indicates that the J_c value at a given field H in the FC state is higher than that in the ZFC state, in good agreement with the isofield ac susceptibility measurements discussed earlier. The observation that the FC magnetization curves eventually merge into the ZFC magnetization curve (i.e., the envelope loop) implies that the more strongly pinned FC vortex state heals to a more ordered ZFC state as the vortex state adjusts to a large enough change ΔH in the external dc field [35]. This change ΔH in the dc field required to anneal a given FC state to a neighbouring ZFC like state also increases as H approaches the peak field H_p , where the lattice is nearly amorphous [7] (ΔH varies from ~ 2 kOe in the PE regime to ~ 80 Oe down to very low field far away from the PE regime). The *overshooting* by the FC magnetization curve is however absent for field cooling in a field $H_i > H_p$ (see Fig. 5). In such a case, the FC magnetization curve readily merges with the reverse envelope curve, since the history effect in J_c disappears at the peak position of the PE, as seen earlier in the temperature dependent ac susceptibility data as well.

**C. CYCLINGS ACROSS THE ONSET AND THE PEAK POSITIONS OF PE:
EVIDENCE FOR SHATTERING OF THE FLL**

I. THERMAL CYCLINGS DURING ISOFIELD AC SUSCEPTIBILITY MEASUREMENTS:

A deeper insight into the path dependence in $\chi'(T)$ can be brought out by performing thermal cyclings across the *onset* and the *peak* positions of PE as it yields striking evidence of the stepwise pulverization of the FLL [23].

The FLL prepared in the ZFC mode, after applying the required field was warmed up to three pre-selected temperatures, T_I , T_{II} and T_{III} , such that, (i) $T_I < T_{pl}$, (ii) $T_{pl} < T_{II} < T_p$ and (iii) $T_p < T_{III} < T_c$. The $\chi'(T)$ responses were then recorded while cooling down in field (FCC) from the above three pre-selected temperatures. The results are illustrated in Fig. 6, where the short-dashed and the solid lines (with data points omitted) are the responses produced in the ZFC and FCW modes, respectively; these were shown earlier in Fig. 3. The cool down curves from the three pre-selected temperatures are represented by specific symbols. The following features are noteworthy in Fig. 6:

(1) For cooling down the sample from a temperature less than the onset of peak effect ($T_I < T_{pl}$), the cool down curve retraces the ZFC warm-up curve, i.e., the changes in the FLL that occur along this path are reversible.

(2) For cooling down from a temperature T_{II} , such that $T_{pl} < T_{II} < T_p$, the $\chi'(T)$ response initially tries to move towards that of the more ordered ZFC state, thereby, effectively retracing the ZFC response. But, suddenly very close to $T = T_{pl}$, i.e., just above the onset of the PE, it undergoes a huge, sharp jump and $\chi'(T)$ drops precipitously to a value more diamagnetic, and hence, the FLL far more disordered than the corresponding state during

the ZFC warm-up cycle. (In fact, the $\chi'(T)$ response just below T_{pl} (during FCC from T_{II}) is even more diamagnetic and thus the FLL more disordered than the corresponding FLL state during the FC warm up cycle.) This sharp jump towards a new, highly disordered state reveals a characteristic hysteretic behavior across the T_{pl} transition. A novel feature of this hysteretic response across T_{pl} is that it is like an open hysteresis loop, i.e., the $\chi'(T)$ response can never by itself (at $T < T_{pl}$) recover to the ZFC like response. On cooling down further, the new $\chi'(T)$ curve (FCC from T_{II}) cuts across the FCW response, thereby, becoming relatively less diamagnetic than the FCW curve down to the lowest temperature ($T \ll T_{pl}$).

(3) When the FLL is cooled down from a temperature above the peak position of the PE ($T_{III} > T_p$), the cool down ac susceptibility response initially appears to retrace the FCW curve down to T_p . But below T_p , the $\chi'(T)$ response becomes more diamagnetic than both the ZFC and FCW responses, thereby creating a vortex state with even still larger J_c value. Between T_p and T_{pl} , this highly disordered state stages a partial recovery. However, near the onset of PE ($\geq T_{pl}$), this partially recovered disordered state has J_c closer to (but larger than) that of the state obtained by cooling down (to $T \leq T_{pl}$) from T_{II} ; but below T_{pl} , it undergoes further disordering (see the curve FCC from T_{III}). It may be noted that eventually at $T \ll T_{pl}$, $\chi'(T)$ response asymptotically merges with the FCW curve.

The above results bear close resemblance with the data in $2H\text{-NbSe}_2$ and CeRu_2 [23] and reaffirm the notion of the stepwise shattering process of the FLL across the temperatures T_{pl} and T_p .

II. CYCLINGS VIA MINOR HYSTERESIS LOOPS IN AN ISOTHERMAL DC MAGNETIZATION EXPERIMENT :

Another interesting manifestation of the path dependent behavior across the onset posi-

tion of PE can be seen in the isothermal dc magnetization hysteresis data via a characteristic feature in the so called minor hysteresis loops, as reported first by Roy and Chaddah [2] in several samples of CeRu₂ and its derivatives [6,36]. It was pointed out [2,6,30,36] that the minor loops initiated from fields lying in between the onset and the peak fields of PE (i.e., for $H_{pl} < H < H_p$), saturate without merging with the reverse envelope loop. We show in Figs. 7(a) and 7(b) the behaviour of minor magnetization curves initiated from fields lying in between H_{pl}^f and H_p at 4.5 K in Ca₃Rh₄Sn₁₃. The expanded data in the main panel of Fig. 7(b) clearly elucidates that the saturated (i.e., the highest) values of the minor loops do not meet the reverse envelope curve (identified by the continuous line). The inset panel of Fig. 7(b) shows how the minor loops eventually merge into the reverse envelope near H_{pl}^r . Note that the difference between the saturated value of a minor curve and the magnetization value on the reverse envelope curve decreases as the field from which the minor loop is initiated approaches the peak field H_p . For fields above H_p , the minor curves readily merge into the reverse envelope curve.

Notionally, above H_p , the $J_c(H)$ values on the forward and reverse legs of the envelope hysteresis loop are just phase reversed, i.e., their magnitudes do not display path dependence. An estimate of the current density values along the forward/reverse portion of the envelope loop between H_{pl}^f/H_{pl}^r and H_p can be made by examining the respective half widths of the magnetization hysteresis loop [35]. The magnetization data of Fig. 7(b) leads to the inference that $J_c^f(H) < J_c^r(H)$ for $H_{pl} < H < H_p$. The inequality $H_{pl}^f < H_{pl}^r$, and the distinct identities of the different members of the family of minor loops in the field interval H_{pl}^r and H_{pl}^f vividly exemplify the irreversibility and the path dependence in the physical phenomenon that occurs across the onset position of the PE along the forward leg.

IV. DISCUSSION

A. SUPERCONDUCTING PARAMETERS OF $\text{Ca}_3\text{Rh}_4\text{Sn}_{13}$:

$\text{Ca}_3\text{Rh}_4\text{Sn}_{13}$ is an isotropic superconductor, well described under the framework of phenomenological Ginzburg-Landau (GL) theory in the isotropic limit. Table 1 summarizes the values of various physical parameters of $\text{Ca}_3\text{Rh}_4\text{Sn}_{13}$ at a temperature of 4.5 K obtained [37] from the ac susceptibility and dc magnetization data using the GL theory. The dimensionless Ginzburg-Landau parameter κ , defined as the ratio of the two characteristic lengths λ and ξ , obtained for this isotropic low T_c superconductor is ≈ 17.5 , whereas the coherence length ξ and the penetration depth λ at 4.5 K are $\sim 130 \text{ \AA}$ and $\sim 2270 \text{ \AA}$, respectively. The presence of disorder, in the forms of thermal fluctuations (dynamic) and the quenched random pinning centres (static), governs the statics and the dynamics of the vortex array. The importance of these two sources of disorder can be quantified [38] by the values of Ginzburg number (G_i), defined as $G_i = (1/2)(k_B T_c / H_c^2 \xi^3 \epsilon)^2$, and the ratio j_c/j_0 , where j_c and j_0 denote the depinning and depairing current densities, respectively. In order to conveniently observe the melting or the amorphization transition of the vortex lattice in any type II superconductor, the following two criteria must be fulfilled. The system must have an appreciably large value of Ginzburg number G_i , which guarantees an adequate separation of the vortex melting/amorphization curve from the H_{c2} line. The system must have sufficiently wide very weakly pinned region well below the superconductor-normal phase boundary, which could help to identify the occurrence of the PE in the magnetization experiments, which is a reliable signature of the process of amorphization of vortex lattice. The Ginzburg number G_i , which measures the relative size of the minimal ($T = 0$) condensation energy $H_c^2(0)\epsilon\xi^3(0)$ within a coherence volume and the critical temperature T_c , for $\text{Ca}_3\text{Rh}_4\text{Sn}_{13}$ is $\sim 10^{-7}$. This value is not too large [1,38] indicating that $\text{Ca}_3\text{Rh}_4\text{Sn}_{13}$ system has a rather narrow critical fluctuation region in (H, T) phase space, where the vortex lattice can undergo melting transition due to thermal fluctuations alone. However, the ratio j_c/j_0 is $\sim 7 \times 10^{-5}$ for weakly pinned $\text{Ca}_3\text{Rh}_4\text{Sn}_{13}$ crystals, which is few orders of magnitude lower than that in the typical crystals of high T_c cuprate systems [1,38]. Such weak pinning in $\text{Ca}_3\text{Rh}_4\text{Sn}_{13}$ crystals can be

conjectured to be a consequence of the absence of generic extended pinning sites, thereby leading to the assumption that pinning is being mainly structural and provided by the point defects in this system. The weak pinning situation is very helpful as the structural and the dynamical behaviour of the vortex array can be studied within the framework of the Larkin-Ovchinnikov (LO) collective pinning theory [39,40]. One can therefore safely assume that FLL in $\text{Ca}_3\text{Rh}_4\text{Sn}_{13}$ is well-formed with large Larkin domains. The small j_c/j_0 ratio makes $\text{Ca}_3\text{Rh}_4\text{Sn}_{13}$ an attractive candidate for the study of pristine phase transitions [38,41–43] of vortex matter in disorder-free context, like, the FLL amorphization transition through the observation of the phenomenon of peak effect [1].

B. COLLECTIVE PINNING DESCRIPTION

The motivation to invoke LO description [39] for explaining the observed behaviour in $\text{Ca}_3\text{Rh}_4\text{Sn}_{13}$ is supported by the field dependence of critical current density in it. $J_c(H)$ can be estimated within the prescription of critical state model [29] using magnetization hysteresis data of Fig. 2 and the knowledge of the dimensions of the crystal [33]. Figure 8 shows $J_c(H)$ vs H behaviour at 4.5 K on a log-log plot. In the ZFC mode, J_c^{ZFC} vs H displays a linear variation in Fig. 8, which amounts to a power law dependence for $J_c(H)$ prior to reaching the PE region at H_{pl} . Such a power law dependence is often taken to be a signature of collectively pinned elastic solid [44]. Figure 8 also includes the current density in the FC state estimated using the saturated values of minor hysteresis curves initiated from different $M_{FC}(H)$ values. The difference between the highest magnetization value on the minor hysteresis curve initiated from a given H and the notional equilibrium magnetization value could be taken as a measure of $J_c^{FC}(H)$ [35]. It is apparent from Fig.8 that the difference between $J_c^{FC}(H)$ and $J_c^{ZFC}(H)$ values decreases as H decreases such that at a field of about 4 kOe, one cannot distinguish between the FC and ZFC vortex states on the basis of their critical current density values. A similar trend was noted [26] in a crystal

of $2H$ -NbSe₂, where the difference between the J_c values in FC and the ZFC states ceased at about 1 kOe. It is noteworthy to recall here that in another study [45] on a variety of $2H$ -NbSe₂ crystals, it was demonstrated that the structure in the PE and thermomagnetic history effects in $\chi'(T)$ data correlate with effective pinning in a manner that the first drop in $\chi'(T)$ at T_{pl} is pinning induced. For a given amount of quenched disorder, the effective pinning increases as H increases. We explored this notion in Ca₃Rh₄Sn₁₃ as well via the study of $\chi'(T)$ response in ZFC and FC states in a field of 5.3 kOe and its comparison with the data recorded in higher dc fields. Figure 9 summarizes the $\chi'(T)$ data recorded at 5.3 kOe. It can be noted that there is only a tiny difference between ZFC and FC curves at $T \ll T_{pl}$. The inset in Fig. 9 shows how the difference between the ZFC and the FC data, along with the structure in the PE across T_{pl} and T_p , has become less prominent at 5.3 kOe as compared to the behaviour displayed in Fig. 1(c) for 10 kOe.

Within the frame work of LO model, the presence of quenched random disorder in the elastic FLL destroys the perfect long range order of the FLL through a competition between the interaction (i.e., the rigidity of the FLL) and the randomness leading to a limited spatial region within which the FLL remains well formed. The macroscopic critical current density J_c in the presence of pinning is given by the pinning force equation [39,40]:

$$F_p = J_c H = (W/V_c)^{1/2} = [n_p \langle f_p^2 \rangle / R_c^2 L_c]^{1/2}, \quad (2)$$

where W and V_c represent the pinning parameter and the correlation volume of a Larkin domain within which the FLL is undistorted and well correlated despite the presence of pinning. In the above equation, n_p is the density of pinning centers (pins), f_p is the elementary pinning interaction proportional to the condensation energy and R_c and L_c are collective pinning radial and longitudinal correlation lengths. The correlation lengths depend on both the elasticity of the FLL as well as pinning, characterized by the parameter W , and are given by,

$$R_c = [c_{44}^{1/2} c_{66}^{3/2} r_f] / W$$

$$\text{and } L_c = [c_{44}/c_{66}]^{1/2} R_c, \quad (3)$$

where c_{44} and c_{66} are the tilt and the shear moduli of the FLL, respectively, and r_f is the range of interaction of the pinning force. In the LO theory, the pinning interaction can only decrease with increasing T , which corresponds only to a monotonic decrease in J_c with increasing T . Thus, the anomalous increase in J_c at the PE can be rationalized in the LO scenario only by an introduction of an anomalous sudden drop in the Larkin volume V_c . The two discontinuous jumps in the current density J_c at T_{pl} and T_p in $\chi'(T)$ data, therefore, imply a sudden shrinkage of V_c at T_{pl} and T_p . This picture proposes that for a sample with substantial pinning, the competition between interaction and disorder leads to some threshold behaviours. When the pinning energy overcomes the elastic energy of the FLL, which is continuously softened due to increase in T , a disorder induced transition transforms the FLL from an elastic medium to a plastically deformed vortex state with a proliferation of topological defects (dislocations) at the onset of PE corresponding to the first jump in the ac susceptibility response (at T_{pl}) [23]. At a higher temperature, the thermal energy overcomes the elastic energy and the pinning induced shattering transition [23,45] produces a complete amorphization of the vortex solid at the peak position of the PE, which could be identified with the second jump in the diamagnetic response at T_p .

The crucial support for the stepwise fracturing of the FLL comes from the thermal cycling experiments performed on a well ordered FLL generated in a ZFC manner (see Fig. 6). When the temperature increases towards the PE region, the FLL softens, the energy needed to create the dislocations decreases and the lattice spontaneously fractures at T_{pl} . While cooling down from a temperature within the PE pocket, i.e., between T_{pl} and T_p , the FLL is cooled from a partially fractured, plastically deformed state. So the FLL initially tries to heal towards the well ordered ZFC state thereby retracing the ZFC response. But, as the temperature decreases progressively towards T_{pl} , the decrease in strength of thermal fluctuations start to stiffen the FLL thereby building up stresses. The system thus fails to

drive out the dislocations in order to heal back to the ZFC state. Instead, it shatters further to release the stresses and reaches a new metastable state. This characteristic feature also yields an open hysteresis loop, i.e., after the $\chi'(T)$ response has reached the new metastable state, it is unable to recover to the ZFC like response by itself. To reach back to the ZFC state from this metastable state, one needs to shake the FLL vigorously by an external driving force [35]. This characteristic hysteretic behaviour across the T_{pl} transition is definitely novel; it is not usually seen across a typical first order (melting) transition in the absence of disorder.

The differences between the vortex states formed during cool down from $T > T_p$ and those evolving during FCW mode probably originate from the slow dynamics [1,23,26] of the order-disorder transformation across T_{pl} and T_p . We believe that above T_p , the FLL transforms into a completely pulverized state, which is so disordered that the FLL correlations beyond first few nearest neighbour inter-vortex spacings are immaterial. Thus, if the FLL is cooled down from such a disordered state (i.e., $T > T_p$), one cools in liquid-like correlations and the FLL remains in an amorphous state (supercooled state) down to a much lower temperature (than that during field cooled warm up cycle). The above scenario leads us to infer that at T_{pl} , the FLL transforms from a nearly defect-free ordered lattice, such as, a Bragg glass phase [41,42] to a highly defective plastically deformed lattice [41–43,46–49] with full of topological defects analogous to a vortex glass phase. Then at T_p , the vortex glass phase further transforms into a completely amorphous but pinned phase ($J_c \neq 0$), above which the lattice is no longer correlated and loses its history and memory. The vanishing of the pinning occurs at an even higher temperature marked as irreversibility temperature T_{irr} .

The path dependence in $\chi'(T)$ response for $T \ll T_p$ is a thought provoking result. It had been shown by Müller, Takashige and Bednorz [50] that the M_{ZFC} differed from M_{FC} up to T_{irr} , and hence one could produce a hierarchy of states whose bulk magnetization values lie in between M_{ZFC} and M_{FC} . In the ZFC state, one typically establishes the critical state with critical current density $J_c(H)$. The states with magnetization lying in between M_{ZFC} and M_{FC} are in sub-critical state with current densities $J(H) \leq J_c(H)$ [51]. At T_{irr} ,

$J_c(H)$ is considered to approach the depinning limit ($J_c \rightarrow 0$). The magnetic shielding response as measured via $\chi'(H, T)$ of all the states whose magnetization values lie in between M_{ZFC} and M_{FC} is dictated by $J_c(H)$ and is nearly identical, i.e., $\chi'(T)$ does not display any path dependence though the magnetization values are path dependent. On the contrary, we witness a thermomagnetic history dependence in $\chi'(T)$ responses in $\text{Ca}_3\text{Rh}_4\text{Sn}_{13}$ below the peak position of the PE. The FLL states prepared via different paths in the (H, T) phase space produce different $\chi'(T)$ responses. The quenched random disorder appears to pin the vortices into different configurations while preparing the FLL via different routes in the (H, T) plane and this results in the history dependence in the screening responses of the FLL. This path dependence in $\chi'(T)$ further reflects the path dependence in J_c [25,35], which in turn gives the path dependence of the correlation (Larkin) volume of the FLL. This leads us to infer that the ZFC state is perhaps the most ordered state with the lowest J_c and the slowly cooled FC state as the most disordered state with the largest J_c . Hence, one can produce a hierarchy of metastable states whose J_c values lie in between J_c^{ZFC} and J_c^{FC} . The history dependence of $\chi'(T)$ responses disappears at the peak position (T_p) of the PE, presumably due to the fact that the FLL prepared in any manner almost completely amorphizes at the peak position and the vortex system *loses order* in equilibrium.

C. DETERMINATION OF R_c AND L_c BY COLLECTIVE PINNING ANALYSIS

Within the LO framework of collective pinning, the dimensionality (D) of the collective pinning is determined by the relative magnitude of longitudinal correlation length L_c of a Larkin domain with respect to the thickness d of the sample [38–40]. Thus a transition from 3D to 2D behaviour is predicted only when $L_c \geq d/2$. The estimated value of $L_c(0)$ from the j_0/j_c ratio for $\text{Ca}_3\text{Rh}_4\text{Sn}_{13}$ is much smaller than $d/2$ which indicates that the collective pinning in this system is 3D in nature. We estimate the longitudinal and transverse correlation lengths $L_c(H)$ and $R_c(H)$ respectively of the Larkin volume, at 4.5 K, using

various superconducting parameters calculated from isotropic GL theory (cf. Table 1), within the framework of 3D collective pinning.

The pinning parameter $W(H, T)$ which takes into account both the density as well as the strength of pins, can be written in a separable form as [40] :

$$W(H, T) = W_0(T)f(b), \quad (4)$$

where the field dependent part $f(b)$ of the pinning strength W is determined by the relation

$$f(b) = b(1 - b)^2, \quad (5)$$

where b is the reduced field given by $b = B/\mu_0 H_{c2}$. W_0 can be determined from the expression for single vortex pinning [38], i.e.,

$$W_0 = L_c(0)j_c^2(0)\phi_0\mu_0 H_{c2}(T), \quad (6)$$

where ϕ_0 is the flux quantum and $L_c(0)$ is the longitudinal collective pinning length given by,

$$L_c(0) = \xi(0)[j_0(T)/j_c(0)]^{1/2}. \quad (7)$$

The $(j_0(T)/j_c(0))$ ratio for this superconductor is $\sim 10^4$ and the typical values obtained for $L_c(0)$ and W_0 at 4.5 K are $1.6 \mu\text{m}$ and $6 \times 10^{-7} \text{ N}^2/\text{m}^3$. Incorporating the expression of W in the LO expression for collective pinning (Eq. 2), one gets,

$$J_c H = (W_0 b(1 - b)^2 / R_c^2 L_c)^{1/2}. \quad (8)$$

The longitudinal correlation length L_c and the transverse correlation length R_c are again connected by the equation [40] :

$$L_c = (c_{44}/c_{66})^{1/2} R_c \approx (2\sqrt{2}/\pi\xi)(b/1 - b)^{1/2} R_c^2, \quad (9)$$

where c_{66} and c_{44} are the shear and the tilt moduli, respectively, given by,

$$c_{66} \approx [\phi_0 B / 16\pi\mu_0\lambda^2](1 - b)^2 = [\phi_0^2 / 32\pi^2\mu_0\lambda^2\xi^2]b(1 - b)^2. \quad (10)$$

and

$$c_{44}(k_{\perp}, k_z) \approx c_{44}^0 / (1 + \lambda_h^2 k_z^2 + \lambda_h^2 k_{\perp}^2) \approx c_{44}^0 (1 + \lambda_h^2 k_{\perp}^2) \approx c_{44}^0 R_c^2 / \pi^2 \lambda_h^2 \quad (11)$$

by considering $L_c \gg R_c$ where k_{\perp} and k_z are the wave vectors describing the deformation fields normal and parallel to the field direction respectively, $\lambda_h = \lambda / (1 - b)^{1/2}$ is the renormalized length scale [52] of the order parameter λ at large induction B and $c_{44}^0 = B^2 / \mu_0$. Plugging Eq. 9 into Eq. 8, one can obtain the expressions for the two correlation lengths R_c and L_c as,

$$R_c = [(W_0 b (1 - b)^2) / (2\sqrt{2} / \pi \xi (b / (1 - b))^{1/2})]^{1/4} [1 / J_c H]^{1/2} \quad (12)$$

and

$$L_c = [2\sqrt{2} / \pi \xi (b / (1 - b))^{1/2}]^{1/2} [W_0 b (1 - b)^{1/2}]^{1/2} [1 / J_c H]. \quad (13)$$

Figure 10 summarizes the computed data for the field dependence of the ratios R_c/a_0 and L_c/d for the FLL prepared at 4.5 K in ZFC mode as well as in FC mode in the $\text{Ca}_3\text{Rh}_4\text{Sn}_{13}$ crystal under study. For the ZFC mode, both R_c/a_0 and L_c/d initially increase with field upto the onset field H_{pl} of PE. But, between H_{pl} and H_p , they decline rapidly indicating that the elastic energy decays much faster than the pinning energy as R_c and L_c decay faster than the pinning parameter W . Near the peak field H_p of the PE, $R_c/a_0 \rightarrow 1$ which supports the view that the FLL gets completely amorphized as the shear modulus c_{66} goes to zero. However, for the FC state, both R_c/a_0 and L_c/d show weaker variation with H upto $0.8 H_{pl}$, after which they decrease gradually, reaching the amorphous limit near H_p .

D. VORTEX PHASE DIAGRAM

Collating all the ac susceptibility and dc magnetization data (including those from Ref. 24), we can finally construct a vortex phase diagram (see Fig. 11) of the conventional type II superconductor $\text{Ca}_3\text{Rh}_4\text{Sn}_{13}$. In Fig. 11, the lower critical field line $H_{c1}(T)$, below which

the superconductor is in the Meissner state, has been drawn from an analysis of isothermal dc magnetization measurements performed at low fields [37]. The H_{c2} line, above which the system is in normal state, has been drawn from the values obtained from the ac susceptibility as well as dc magnetization data. The regime in the magnetic phase diagram enclosed by these two lines gives the Abrikosov state or the mixed state of a type II superconductor, where the magnetic field penetrates in the form of discrete flux quanta which interact repulsively among themselves to form the FLL. After the discovery of high T_c superconductors, Müeller, Takashige and Bednorz [50] introduced an extra line, designated as an irreversibility line in the mixed state of type II superconductors, which was thought to mark the predominance of the influence of thermal fluctuations on the vortices. In weakly pinned systems, the competition and interplay between the static (quenched random pinning) and dynamic (thermal fluctuations) disorder and the elasticity of the lattice creates a richer phase diagram comprising a few more lines within the Abrikosov phase. These lines reflect how the nearly defect-free (very small j_c/j_0 ratio) elastically deformed vortex lattice undergoes loss of order in steps. The onset of the PE, which is identified with $T_{pl}(H)$ in ac susceptibility data and $H_{pl}(T)$ in dc magnetization data is drawn as (H_{pl}, T_{pl}) line in Fig. 11. This line marks the onset of shattering of the FLL as the pinning energy overcomes the elastic energy and hence, a transition ensues from an elastic solid similar to Bragg glass phase to a plastically deformed vortex state full of topological defects analogous to a vortex glass phase. The shattering of the FLL gets completed at the peak position of the PE (marked as (H_p, T_p)) producing a near collapse of the Larkin domain and complete amorphization of the FLL, thereby, representing a transformation to a highly viscous pinned amorphous state as the elastic energy is completely overcome by the thermal energy. If we choose to identify (H_p, T_p) line in Fig. 11 with the FLL melting curve (B_m, T) relation [38]:

$$B_m = \beta_m (c_L^4 / G_i) H_{c2}(0) (T_c / T)^2 [1 - (T / T_c) - (B_m / H_{c2}(0))]^2, \quad (14)$$

where β_m , G_i and $H_{c2}(0)$ are taken as 5.6 [38], $\sim 1.3 \times 10^{-7}$ and ~ 4.5 T, respectively, the Lindemann number c_L is found to be ~ 0.1 . At a higher field H_{irr} , the critical current

density vanishes as identified by the vanishing of hysteresis in the dc magnetization data. The irreversibility line marks a crossover (presumably dynamic) from a pinned amorphous to an unpinned amorphous state as the thermal energy overcomes the pinning energy.

SUMMARY

In summary, the peak effect, an anomalous upturn in the critical current density of superconductors, has been investigated in detail for the superconducting system $\text{Ca}_3\text{Rh}_4\text{Sn}_{13}$ via isofield ac and isothermal dc magnetization measurements. A structure in the peak effect region, comprising two first-order like jumps at the onset (T_{pl}) and the peak (T_p) positions of the PE, has been observed in the isofield ac susceptibility measurements. Our ansatz about this two-peak structure is that the first peak reflects the commencement of a pinning induced stepwise shattering of the FLL through the sudden shrinkage of the correlation (Larkin) volume V_c at T_{pl} [23,45]. Thermal cycling across the onset temperature T_{pl} reveals an open hysteresis loop across it, which is a spectacular manifestation of the shattering phenomenon of the FLL. The macroscopic current density J_c of $\text{Ca}_3\text{Rh}_4\text{Sn}_{13}$ shows pronounced thermomagnetic history dependence below T_p , which reveals the role played by quenched random disorder on the FLL. The disappearance of history dependence above T_p , reflects the absence of memory of any previous history and the complete amorphization of the FLL. The two-peak structure becomes inconspicuous below a certain dc field indicating a possible cross over from an interaction dominated regime to a pinning dominated regime when lattice constant a_0 becomes comparable to the penetration depth, which measures the range of the electromagnetic interaction between the vortices. Finally, the vortex phase diagram of $\text{Ca}_3\text{Rh}_4\text{Sn}_{13}$ is constructed which shows close resemblance to phase diagrams drawn earlier for CeRu_2 and $2H\text{-NbSe}_2$ [23]. This could further lead to the establishment of a generic phase diagram for all conventional low- T_c type II superconductors in the presence of quenched random disorder and thermal fluctuations.

REFERENCES

- [1] S. Bhattacharya and M. J. Higgins, Phys. Rev. Lett. **70**, 2617 (1993); M. J. Higgins and S. Bhattacharya, Physica C **257**, 232 (1996) and references therein.
- [2] A. D. Huxley, C. Paulsen, O. Laborde, J. L. Tholence, D. Sanchez, A. Junod and R. Calemczuk, J. Phys. Condens. Matter **5**, 7709 (1993); S. B. Roy and P. Chaddah, *ibid.* **9**, L625 (1997).
- [3] R. Modler, P. Gegenwart, M. Lang, M. Deppe, M. Weiden, T. Luhmann, C. Geibel, F. Steglich, C. Paulsen, J. L. Tholence, N. Sato, T. Komatsubara, Y. Onuki, M. Tachiki and S. Takahashi, Phys. Rev. Lett. **76**, 1292 (1996).
- [4] M. Tachiki, S. Takahashi, P. Gegenwart, M. Weiden, M. Lang, C. Geibel, F. Steglich, R. Modler, C. Paulsen and Y. Onuki, Z. Phys. B **100**, 369 (1996).
- [5] N. R. Dilley, J. Herrmann, S. H. Han, M. B. Maple, S. Spagne, J. Diederichs and R. E. Sager, Physica C **265**, 150 (1996).
- [6] S. B. Roy, Phil. Mag. **65**, 1453 (1992); K. Yagasaki, M. Hedo and T. Nakama, J. Phys. Soc. Jpn. **62**, 3825 (1993); S. B. Roy, P. Chaddah and S. Chaudhary, J. Phys. Condens. Matter **10**, 4885 (1998).
- [7] P. L. Gammel, U. Yaron, A. P. Ramirez, D. J. Bishop, A. M. Chang, R. Ruel, L. N. Pfeiffer and E. Bucher, G. D'Anna, D. A. Huse, K. Mortensen, M. R. Eskildsen, P. H. Kes, Phys. Rev. Lett. **80**, 833 (1998).
- [8] M. Isino, T. Kobayashi, N. Toyota, T. Fukase and Y. Muto, Phys. Rev. B **38**, 4457 (1988).
- [9] J. G. Park, M. Ellerby, K. A. McEwen and M. de Podesta, J. Magn. Magn. Mater. **140-144**, 2057 (1995).
- [10] U. Yaron, P. L. Gammel, D. A. Huse, R. N. Kleiman, C. S. Oglesby, E. Bucher, B.

- Batlogg, D. J. Bishop, K. Mortensen, K. Clausen, C. A. Bolle and F. de la Cruz, Phys. Rev. Lett. **73**, 2748 (1994).
- [11] C. A. Bolle, F. de la Cruz, P. L. Gammel, J. V. Waszczak and D. J. Bishop, Phys. Rev. Lett. **71**, 4039 (1993); F. Pardo, F. de la Cruz, P. L. Gammel, C. S. Oglesby, E. Bucher, B. Batlogg and D. J. Bishop, Phys. Rev. Lett. **78**, 4633 (1997).
- [12] H. Sato, Y. Akoi, H. Sugawara and T. Fukahara, J. Phys. Soc. Jpn. **64**, 3175 (1995).
- [13] C. V. Tomy, G. Balakrishnan and D. Mck. Paul, Physica C **280**, 1 (1997).
- [14] K. Hirata et al., *Advances in Superconductivity VIII*, edited by H. Hayakawa and Y. Enomoto (Springer-Verlag, Berlin, Germany, 1996) p. 619.
- [15] X. Ling and J. I. Budnick, *Magnetic Susceptibility of Superconductors and other Spin Systems*, edited by R. A. Hein, T. L. Francavilla and D. H. Liebenberg (Plenum Press, New York, 1991), p.377.
- [16] G. D'Anna, W. Benoit, W. Sadowski and E. Walker, Europhys. Lett. **20**, 167 (1992); H. K pfer, T. Wolf, C. Lessing, A. A. Zhukov, X. Lancon, R. Meir-Hirman and W. Sch Phys. Rev. B **58**, 2886 (1998) and references therein.
- [17] A. B. Pippard, Philos. Mag. **19**, 217 (1969); A. M. Campbell and J. E. Evetts, Adv. Phys. **21**, 327 (1972) and references therein.
- [18] P. Fulde and R. A. Ferrel, Phys. Rev. **135A**, 550 (1964).
- [19] A. I. Larkin and Y. N. Ovchinnikov, Sov. Phys. JETP **20**, 762 (1965).
- [20] K. Gloos, R. Modler, H. Schimanski, C. D. Bredl, C. Geibel, F. Steglich, A. I. Buzdin, N. Sato and T. Komatsubara, Phys. Rev. Lett. **70**, 501 (1993); A. Ishiguro, A. Sawada, Y. Inada, J. Kimura, M. Suzuki, N. Sato and T. Komatsubara, J. Phys. Soc. Jpn. **64**, 378 (1995).
- [21] G. W. Crabtree, M. B. Maple, W. K. Kwok, J. Herrmann, J. A. Fendrich, N. R. Dilley

- and S. H. Han, *Physics Essays* **9**, 628 (1996).
- [22] C. Tang, X. S. Ling, S. Bhattacharya and P. M. Chaikin, *Europhys Lett.* **35**, 597 (1996) and references therein.
- [23] S. S. Banerjee, N. G. Patil, S. Saha, S. Ramakrishnan, A. K. Grover, S. Bhattacharya, G. Ravikumar, P. K. Mishra, T. V. C. Rao, V. C. Sahni, M. J. Higgins, E. Yamamoto, Y. Haga, M. Hedo, Y. Inada and Y. Onuki, *Phys. Rev. B.* **58**, 995 (1998).
- [24] C. V. Tomy, G. Balakrishnan and D. McK. Paul, *Phys. Rev. B* **56**, 8346 (1997).
- [25] G. Ravikumar, V. C. Sahni, P. K. Mishra, T. V. C. Rao, S. S. Banerjee, A. K. Grover, S. Ramakrishnan, S. Bhattacharya, M. J. Higgins, E. Yamamoto, Y. Haga, M. Hedo, Y. Inada and Y. Onuki, *Phys. Rev. B* **57**, R11069 (1998).
- [26] W. Henderson, E. Y. Anderi, M. J. Higgins and S. Bhattacharya, *Phys. Rev. Lett.* **77**, 2077 (1996); **80**, 381 (1998).
- [27] S. Ramakrishnan, S. Sundaram, R. S. Pandit and G. Chandra, *J. Phys. E* **18**, 650 (1985).
- [28] G. Ravikumar, T. V. C. Rao, P. K. Mishra, V. C. Sahni, S. S. Banerjee, A. K. Grover, S. Ramakrishnan, S. Bhattacharya, M. J. Higgins, E. Yamamoto, Y. Haga, M. Hedo, Y. Inada and Y. Onuki, *Physica C* **276**, 9 (1997); **298**, 122 (1998).
- [29] C. P. Bean, *Rev. Mod. Phys.* **36**, 31 (1964).
- [30] S. Kokkaliaris, D. A. J. de Groot, S. N. Gordeev, A. A. Zhukov, R. Gagnon and L. Taillefer, *Phys. Rev. Lett.* **82**, 5116 (1999).
- [31] A. Huxley, R. Cubitt, D. McK. Paul, E. Forgan, M. Nutley, H. Mook, M. Yethiraj, P. Lejay, D. Caplan and J. M. Penisson, *Physica B* **223** , **224** 169 (1996).
- [32] J. A. Mydosh, *Spin Glasses : An Experimental Introduction*, Taylor and Francis, London, U.K., 1993.

- [33] P. Chaddah, in *Studies in High Temperature Superconductors*, edited by A. V. Narlikar, Nova Science Inc., Comack, NY, USA, 1995, Vol. **14**, pp 245-274.
- [34] A. K. Grover, in *Studies in High Temperature Superconductors*, edited by A. V. Narlikar, Nova Science Inc., Comack, NY, USA, 1995, Vol. **14**, pp 185-244.
- [35] S. S. Banerjee, N. G. Patil, S. Ramakrishnan, A. K. Grover, S. Bhattacharya, G. Ravikumar, P. K. Mishra, T. V. C. Rao, V. C. Sahni and M. J. Higgins, *Appl. Phys. Lett.* **74**, 126 (1999).
- [36] S. B. Roy, P. Chaddah, S. Chaudhary and L. F. Cohen, *Proceedings of the 41st Annual DAE Solid State Physics Symposium, Universities Press, Hyderabad (India)* **41**, 367 (1998).
- [37] S. Sarkar et al., unpublished.
- [38] G. Blatter, M. V. Feigel'man, V. B. Geshkenbein, A. I. Larkin and V. M. Vinokur, *Rev. Mod. Phys.* **66**, 1125 (1994).
- [39] A. I. Larkin and Y. N. Ovchinnikov, *Sov. Phys. JETP* **38**, 854 (1974); A. I. Larkin, *J. Low. Temp. Phys.* **34**, 409 (1979).
- [40] R. Wordenweber, P. H. Kes and C. C. Tsuei, *Phys. Rev. B* **33**, 3172 (1986); L. A. Angurel, F. Amin, M. Polichetti, J. Aarts and P. H. Kes, *Phys. Rev. B* **56**, 3425 (1997).
- [41] T. Giamarchi and P. Le. Doussal, *Phys. Rev. Lett.* **72**, 1530 (1994).
- [42] T. Giamarchi and P. Le. Doussal, *Phys. Rev. B* **52**, 242 (1995).
- [43] M. Gingras and D. A. Huse, *Phys. Rev. B* **53**, 15193 (1996).
- [44] A. Durate, E. F. Righi, C. A. Bolle, F. de la Cruz, P. L. Gammel, C. S. Oglesby, E. Bucher, B. Batlogg and D. J. Bishop, *Phys. Rev. B* **53**, 11336, (1996).
- [45] S. S. Banerjee, N. G. Patil, S. Ramakrishnan, A. K. Grover, S. Bhattacharya, G. Raviku-

- mar, P. K. Mishra, T. V. C. Rao, V. C. Sahni, M. J. Higgins, C. V. Tomy, G. Balakrishnan and D. McK. Paul, Phys. Rev. B **59**, 6043 (1999).
- [46] S. Bhattacharya and M. J. Higgins, Phys. Rev. B **43**, 10005 (1995).
- [47] S. Bhattacharya and M. J. Higgins, Phys. Rev. B **52**, 64 (1995).
- [48] S. Ryu, M. Hellerquist, S. Doniach, A. Kapitulnik and D. Stroud, Phys. Rev. Lett. **77**, 5114 (1997).
- [49] M. C. Faleski, M. C. Marchetti and A.A. Middleton, Phys. Rev. B **54**, 12427 (1996).
- [50] K. A. Müller, M. Takashige and J. G. Bednorz, Phys. Rev. Lett. **58**, 1143 (1987).
- [51] P. Chaddah and G. Ravikumar, Pramana - J. Phys. **31**, L141 (1988).
- [52] E. H. Brandt, J. Low. Temp. Phys. **26**, 709 (1977); **26**, 735 (1977); **28**, 263 (1977); **28**, 291 (1977).
- [53] V. M. Vinokur, P. H. Kes and A. E. Koshelev, Physica C **248**, 179 (1995).

FIGURES

FIG. 1. (a),(b),(c) Isofield ac susceptibility data for various fixed dc bias fields, superimposed with an ac field of amplitude 1 Oe (r.m.s) at a frequency of 211 Hz, maintained parallel to [001] plane of a single crystal of $\text{Ca}_3\text{Rh}_4\text{Sn}_{13}$. Figure 1(a) demonstrates that for dc fields of 0 Oe (i.e., earth's field) and 2.5 kOe, $\chi'(T)$ response exhibits monotonic decrease with T. However, in the upper panel of Fig.1(b), for a dc field of 3.5 kOe, the monotonic decrease of $\chi'(T)$ response is interrupted suddenly, giving rise to an anomalous dip just before $T_c(H)$. The lower panel of Fig.1(b) sketches how the single dip-like feature transforms to a two peak structure, occurring at the *onset* (T_{pl}) and the *peak* (T_p) positions of the peak effect, as the dc bias field is increased further to 5 kOe. Figure 1(c) shows how the structure in the PE regime gets more prominent as one progresses to higher dc fields of 7 kOe and 10 kOe. The inset of Fig. 1(c) shows the T_{pl} and T_p lines, plotted in the thermomagnetic (H, T) phase space.

FIG. 2. The main panel shows the isothermal dc magnetization hysteresis data at 4.5 K obtained via Quantum Design Inc. SQUID Magnetometer system over a scan length of 4 cm with the usual full Scan (FS) method and a new *half scan technique* (HST). H_{pl}^f and H_{pl}^r identify the field values at which PE notionally commences on the forward leg and terminates on the reverse leg, respectively. The peak field of the peak effect, the irreversibility field (where magnetization hysteresis bubble collapses) and the upper critical field are marked as H_p , H_{irr} and H_{c2} , respectively. The two insets in Fig.2 show the magnetization measurements at 6.1 K using HST as well as conventional FS technique. No hysteresis bubble in the magnetization data a la PE is observed for the FS method, whereas the HST, which circumvents the problem of field inhomogeneity, produces measurable magnetization hysteresis in the PE regime. Also, the main panel of Fig. 2 focusses onto a comparison between the two magnetization bubbles measured at 4.5 K by conventional FS method and HST. Besides other differences in the two loops, note that the loop via HST is open before the onset field H_{pl} .

FIG. 3. Temperature dependence of the in phase ac susceptibility data recorded at $H = 10$ kOe for two thermomagnetic histories, namely, zero field cooled(ZFC) and field cooled(FC). In the latter case, the data were recorded during warm-up cycle (FCW). Note that the jumps in $\chi'(T)$ are observed at T_{pl} and T_p in both the plots, and just above T_p , the two curves merge into each other.

FIG. 4. (a),(b) Frequency and amplitude dependence of the isofield ac susceptibility measurements for a FLL prepared by a dc bias field of 10 kOe. Figure 4(a) shows the $\chi'(T)$ responses for two different frequencies of 21 Hz and 211 Hz, whereas Fig. 4(b) shows a comparison of data obtained at two different amplitudes of ac field keeping the frequency invariant. Note that $T_{pl}(H)$ and $T_p(H)$ values in $H = 10$ kOe do not show measurable differences over the limited ranges of the frequency and the amplitude investigated.

FIG. 5. Magnetization hysteresis curves obtained at 4.5 K after field cooling the crystal to different preselected fields. $M_{FC}(H)$ denotes the notional field cooled magnetization value at a given H . Note that the minor magnetization curves can be obtained by either increasing or decreasing the field from a given $M_{FC}(H)$. The field cooled minor magnetization curves so obtained initially cut across the envelope magnetization loop (marked by thin continuous line). The FC minor curves eventually proceed towards the envelope loop. Note that the characteristic behavior which amounts to a FC minor curve of cutting across the envelope curve ceases as H approaches the peak field H_p . Above H_p , the FC minor curve readily merges into the envelope loop.

FIG. 6. Thermal cycling across the onset (T_{pl}) and the peak (T_p) positions of the peak effect in temperature dependent ac susceptibility data. The short-dashed and the solid lines represent the $\chi'(T)$ responses for the ZFC and the FCW states, respectively, which were displayed earlier in Fig.3. T_I , T_{II} and T_{III} identify the temperatures upto which the sample was warmed up each time after preparing the FLL in ZFC mode in a dc bias field of 10 kOe. Thermal cycling was then performed by cooling down (FC) from these three preselected temperatures.

FIG. 7. (a),(b) Minor hysteresis curves generated by decreasing the field from the forward branch of the envelope loop at a fixed temperature of 4.5 K. The minor curves initiated from fields lying in between H_{pl} and H_p do not merge with the reverse leg of the envelope hysteresis loop, this gets clearly demonstrated in the expanded version of the data in the main panel of Fig. 7(b). The inset of Fig. 7(b) shows that the minor magnetization loops eventually merge into each other near H_{pl}^r on the reverse leg on the envelope magnetization loop.

FIG. 8. J_c vs H behaviour for the FLL prepared in the ZFC and FC modes at $T = 4.5$ K, shown on a log-log plot. On the log-log scale, J_c^{ZFC} displays a linear behaviour, which accounts to a power law variation with an exponent of ~ -1 (i.e., $J_c^{ZFC} \sim 1/H$). Such a power law dependence points to a collectively pinned elastic solid and hence the marked region in the (H, T) phase space describes the elastically pinned state of vortex matter. Note that the differences between the FC and ZFC critical current density values vanish at the peak position of the PE.

FIG. 9. $\chi'(T)$ responses obtained for a fixed dc bias field of 5.3 kOe in ZFC and FCW modes. The screening diamagnetic responses for the FLL states prepared in ZFC and FC modes at such low fields show very little differences. The inset focusses onto the two jumps across T_{pl} and T_p values, which are much smaller than the jumps observed for the applied dc bias field of 10 kOe.

FIG. 10. Computed values of radial length R_c/a_0 and longitudinal length L_c/d for $\text{Ca}_3\text{Rh}_4\text{Sn}_{13}$ at $T = 4.5$ K for FLL prepared in ZFC as well as in FC mode. a_0 represents the lattice constant ($\approx \phi_0/\sqrt{B}$) and d denotes the thickness of the sample in the direction of the field. The two ratios for the ZFC mode initially increase with increasing H upto the onset field H_{pl} , where they start decreasing sharply with H . At $H = H_p$, $R_c \sim a_0$, which indicates that the FLL gets completely amorphized at the peak of the PE with the the total loss of radial correlation.

FIG. 11. Vortex phase diagram for $\text{Ca}_3\text{Rh}_4\text{Sn}_{13}$ depicting (H_{pl}, T_{pl}) , (H_p, T_p) , (H_{irr}, T_{irr}) , (H_{c2}, T_c) lines. For an explanation of nomenclature of vortex phases in different (H, T) regions, see text.

TABLES

TABLE I. Superconducting parameters of $\text{Ca}_3\text{Rh}_4\text{Sn}_{13}$ using isotropic GL theory at $T = 4.5 \text{ K}$

$\lambda(\text{\AA})$	κ	$\xi(\text{\AA})$	$H_{c1}(\text{Oe})$	$H_{c2}(\text{Oe})$	$H_c(\text{Oe})$	Gi	$j_0(\text{A/m}^2)$	$j_c(\text{H} = 0)(\text{A/m}^2)$
2270	17.5	130	110	19500	800	3×10^{-7}	1.5×10^{11}	10^7

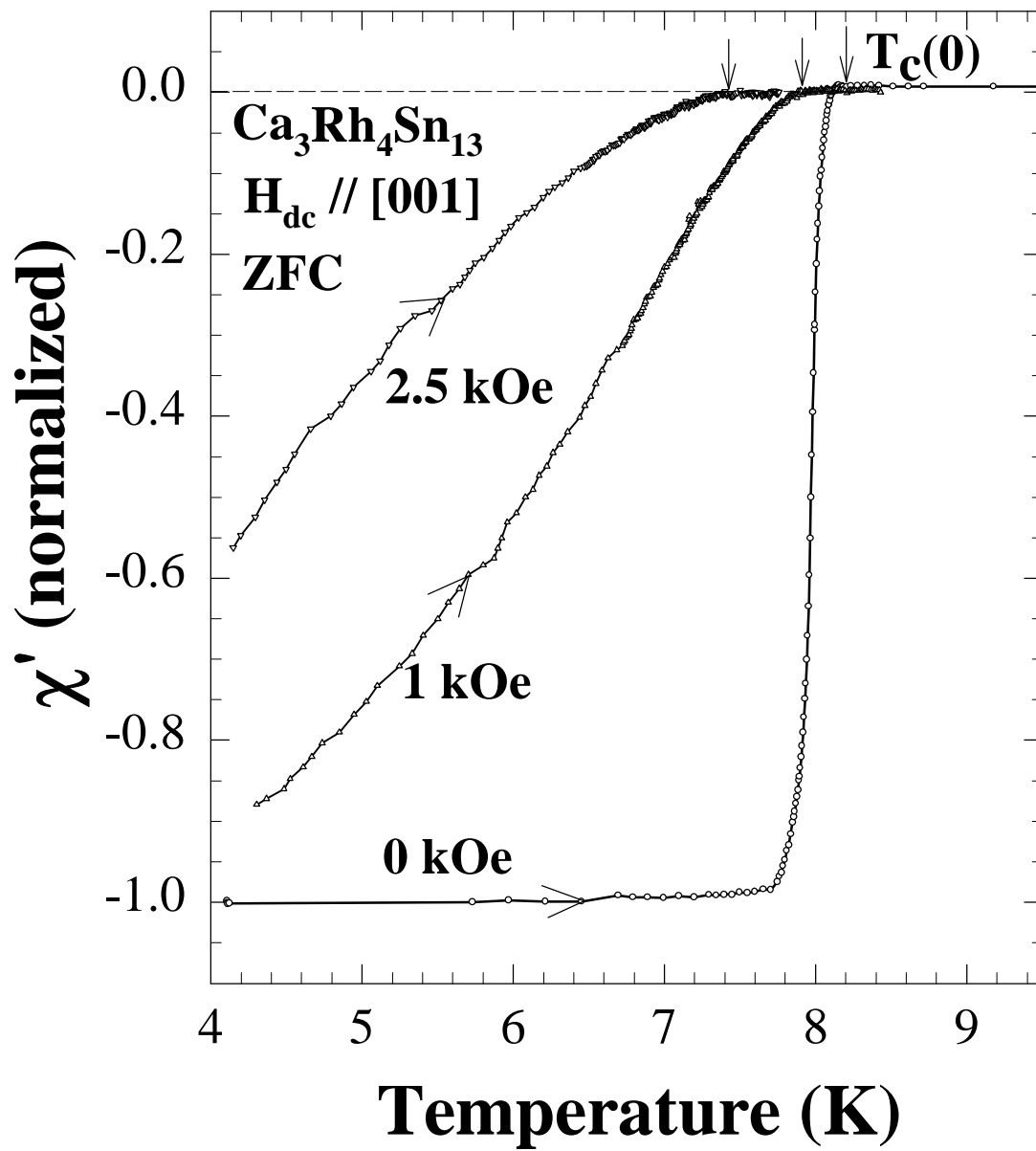


Fig. 1(a) Sarkar et al.

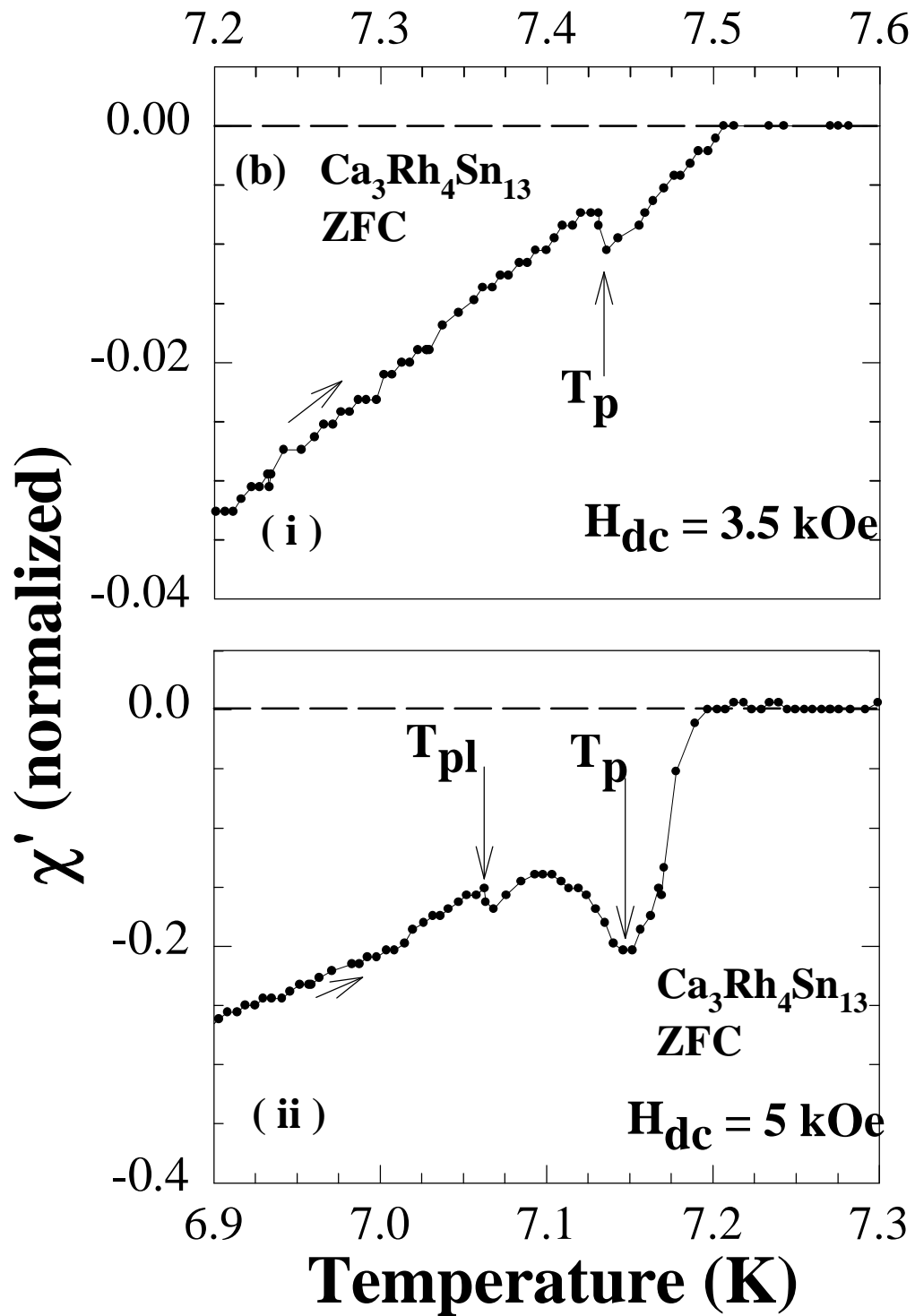


Fig. 1(b) Sarkar et al

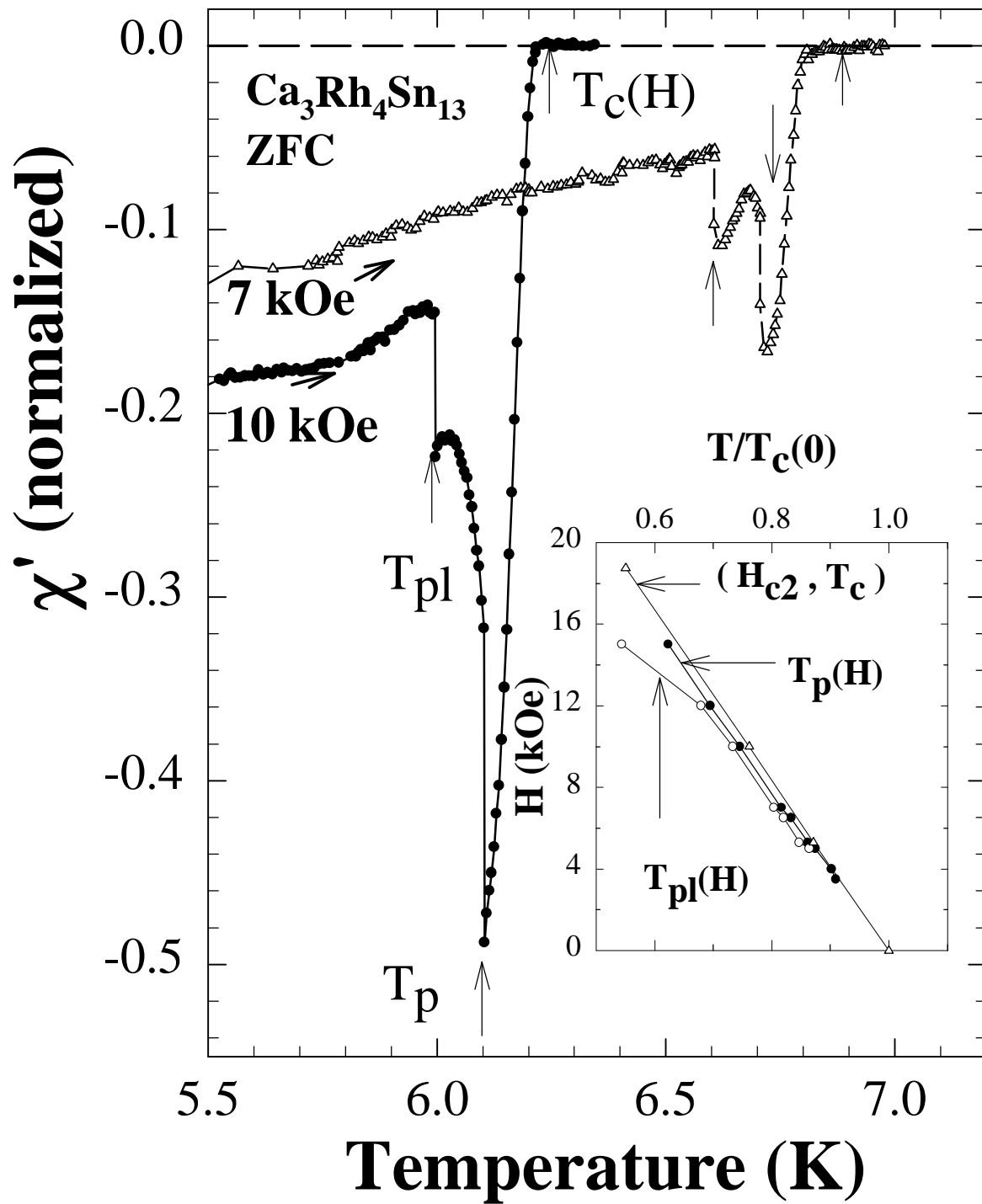


Fig. 1(c). Sarkar et al

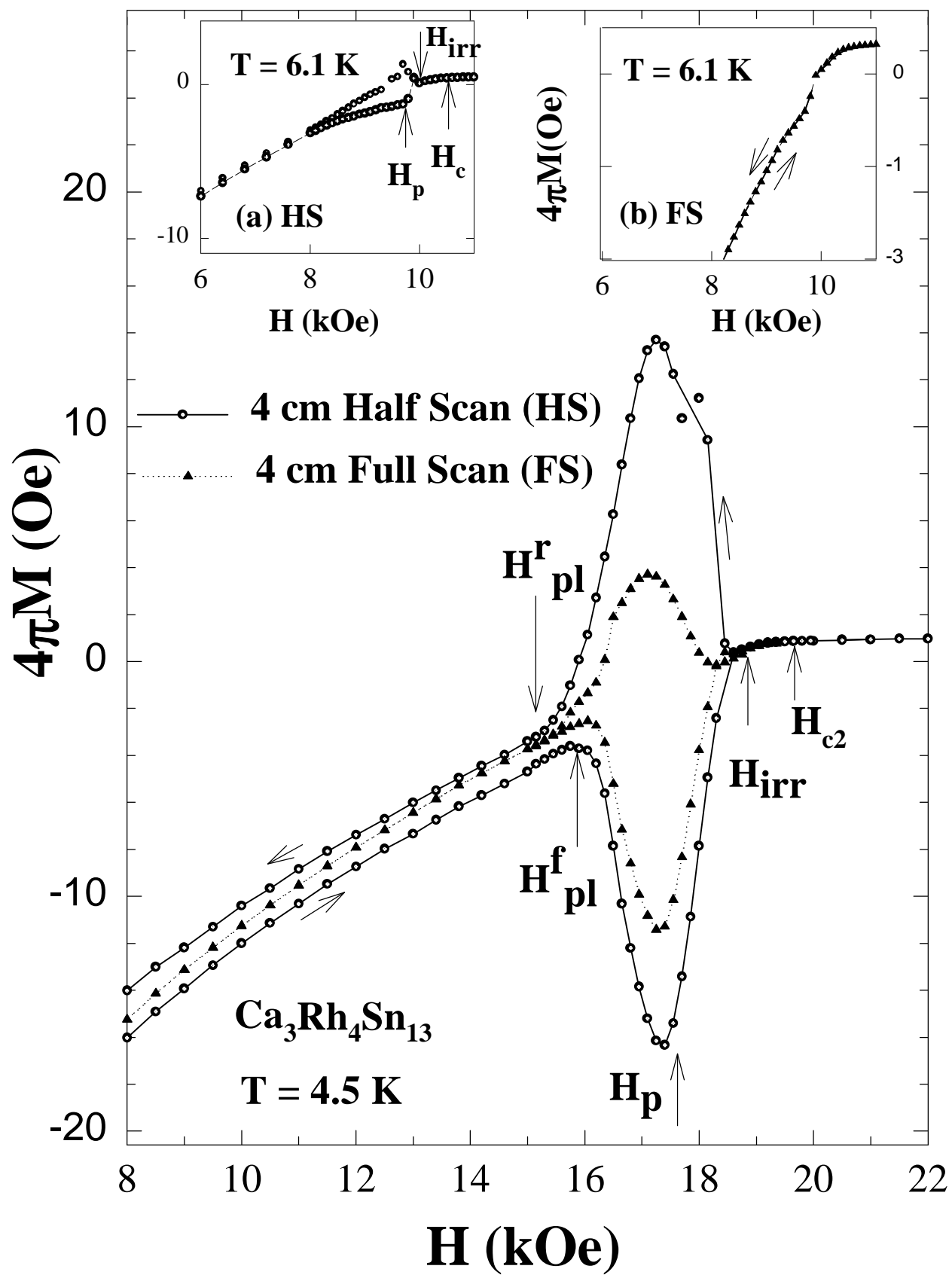


Fig. 2 Sarkar et al

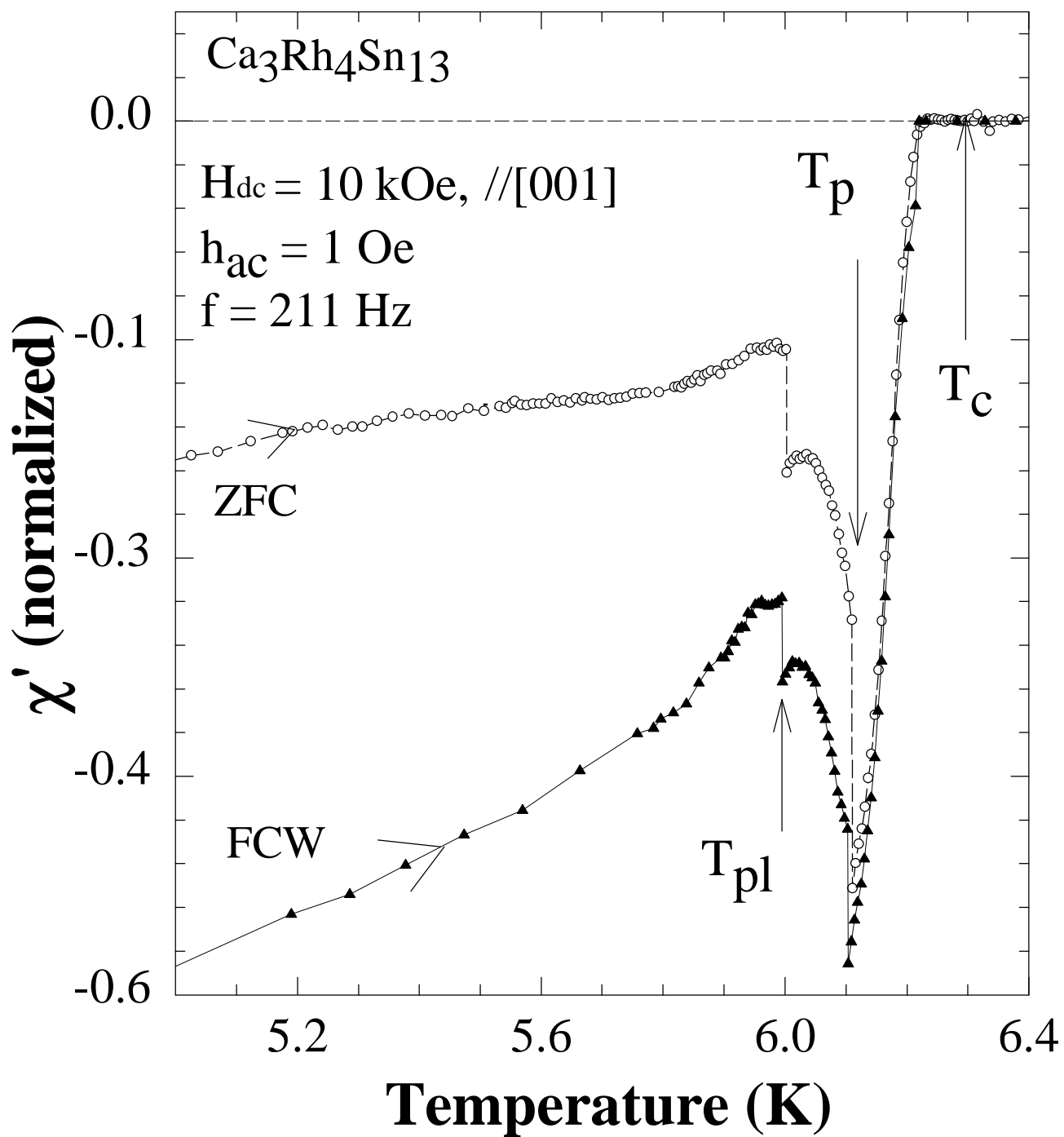


Fig. 3 Sarkar et al

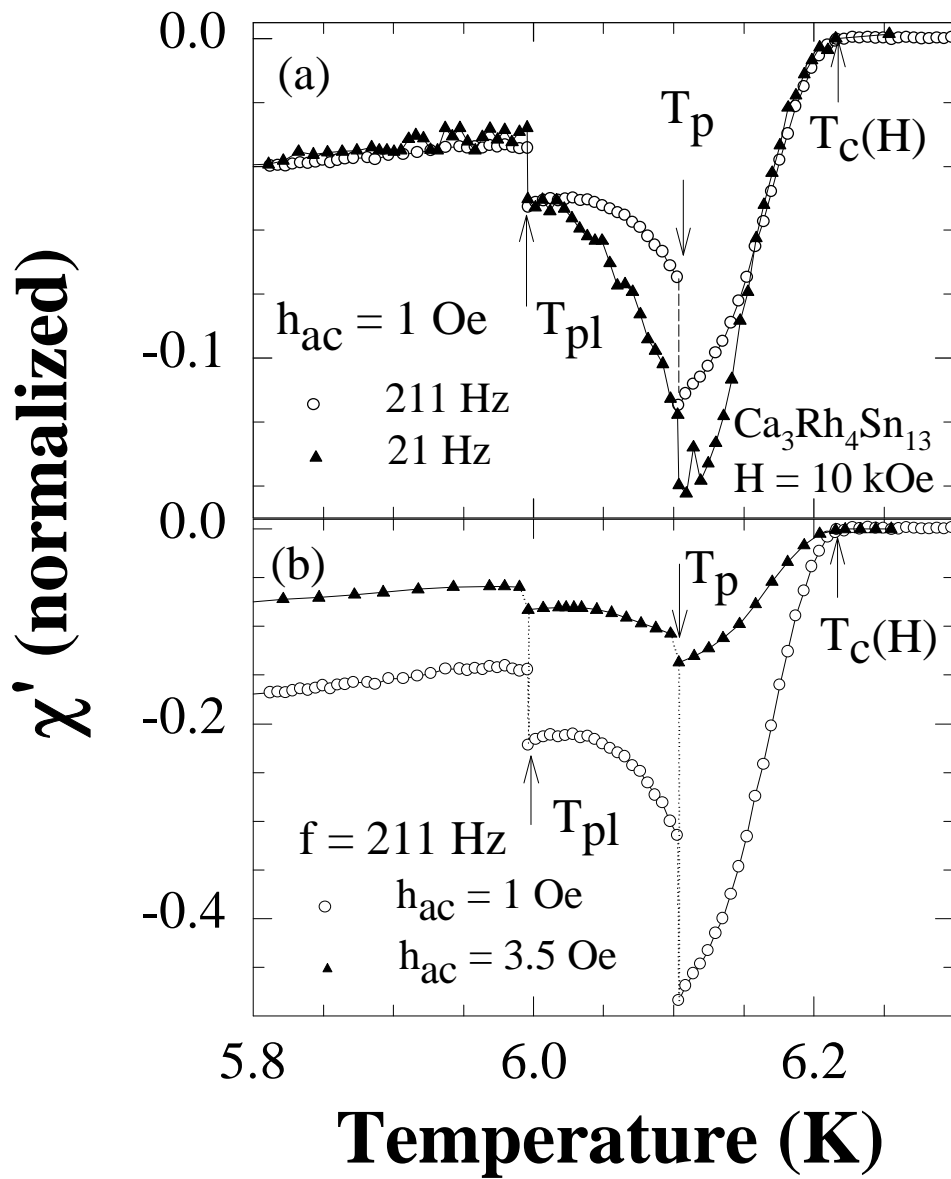


Fig. 4 Sarkar et al

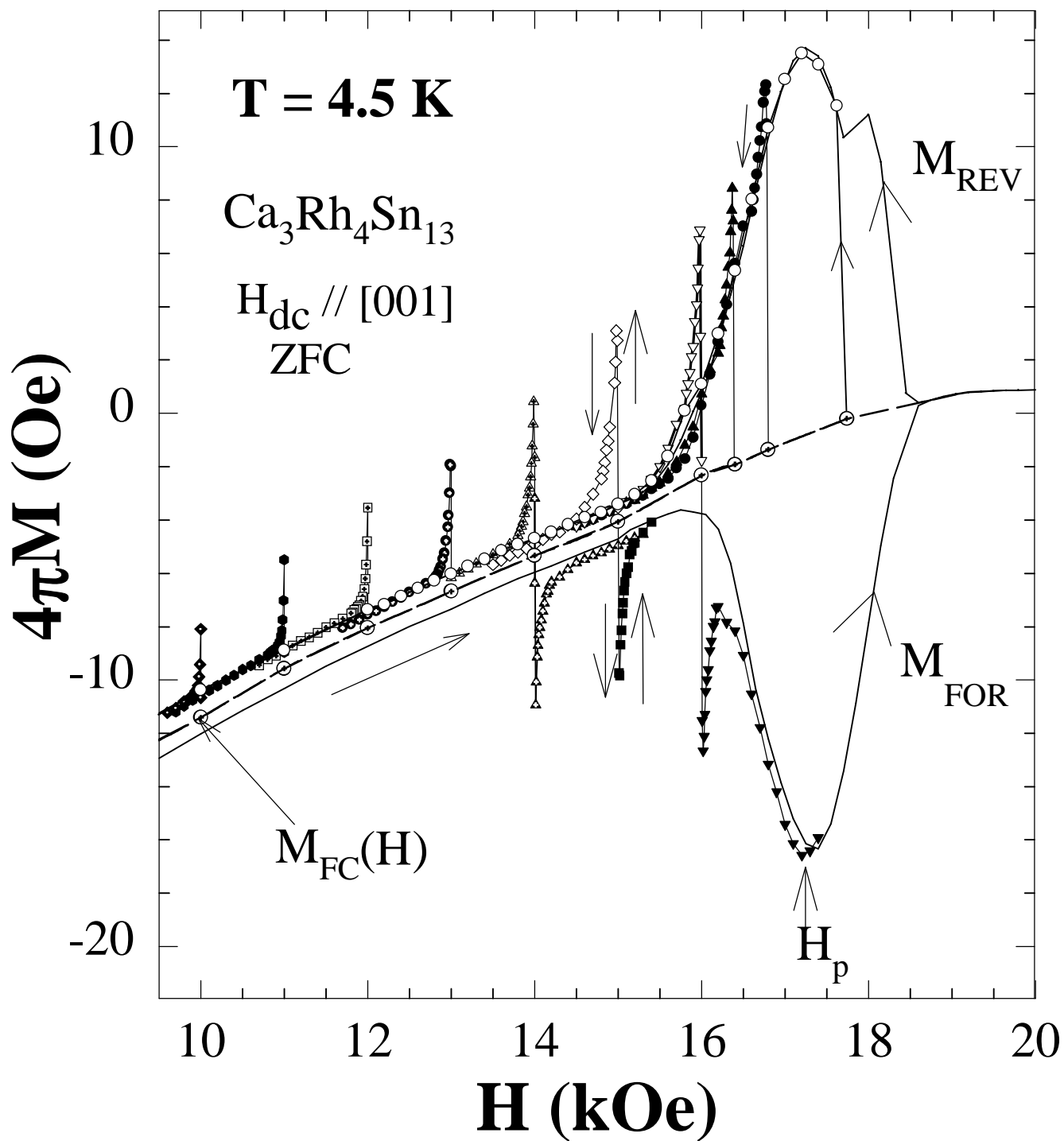


Fig. 5 Sarkar et al

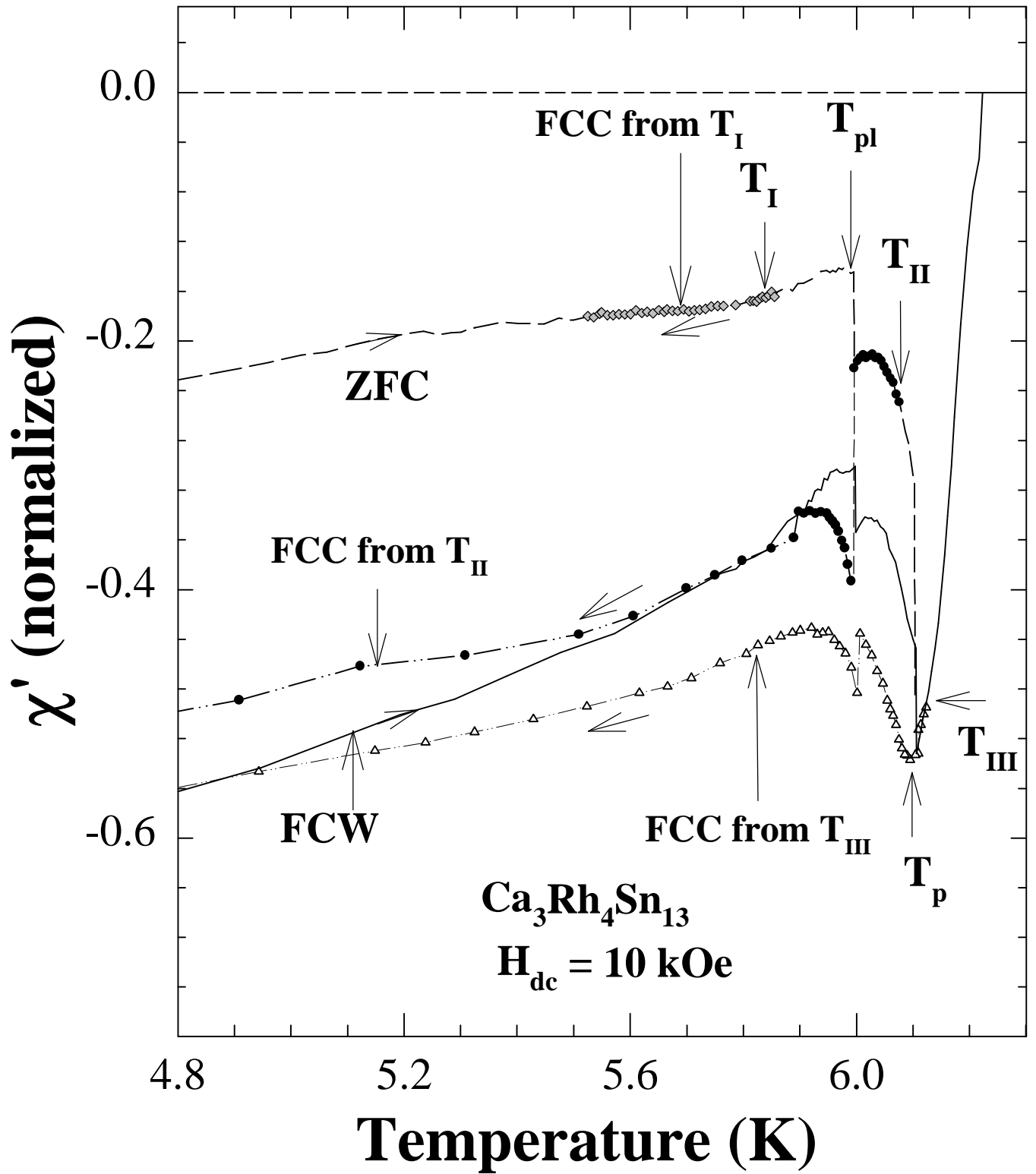


Fig. 6. Sarkar et al

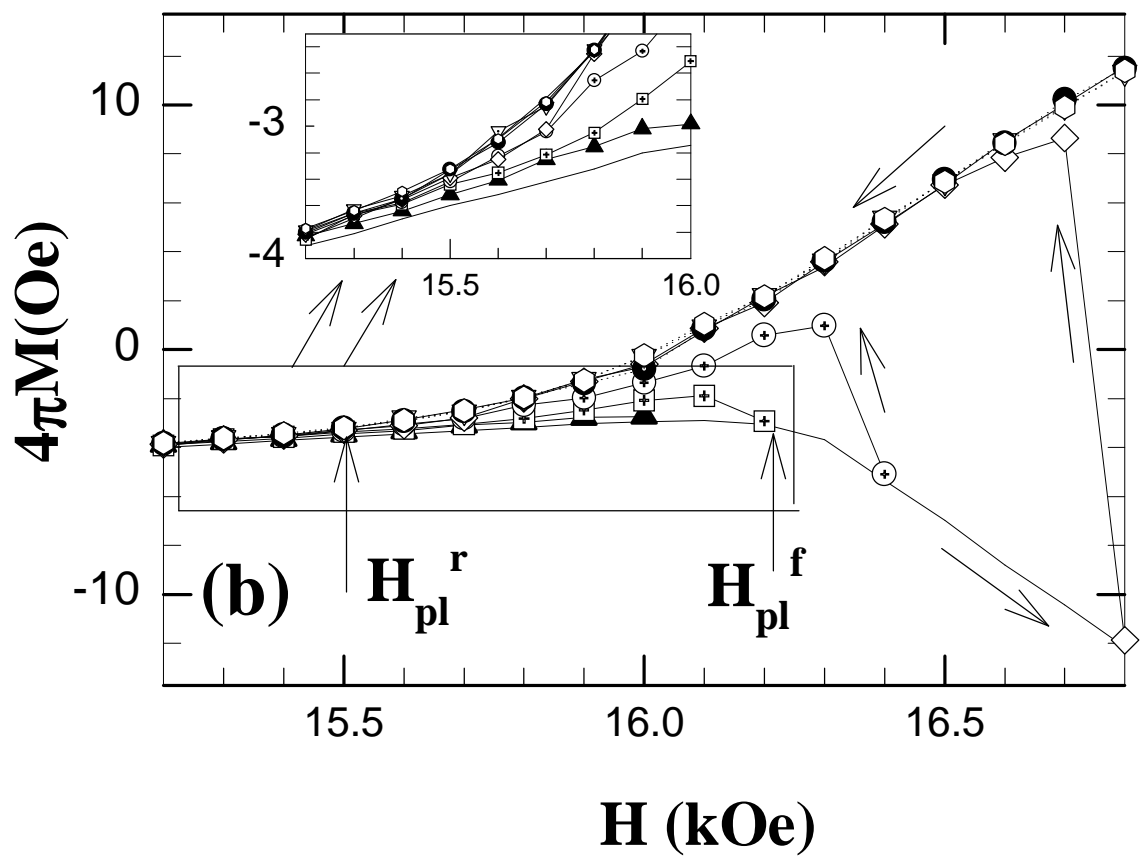
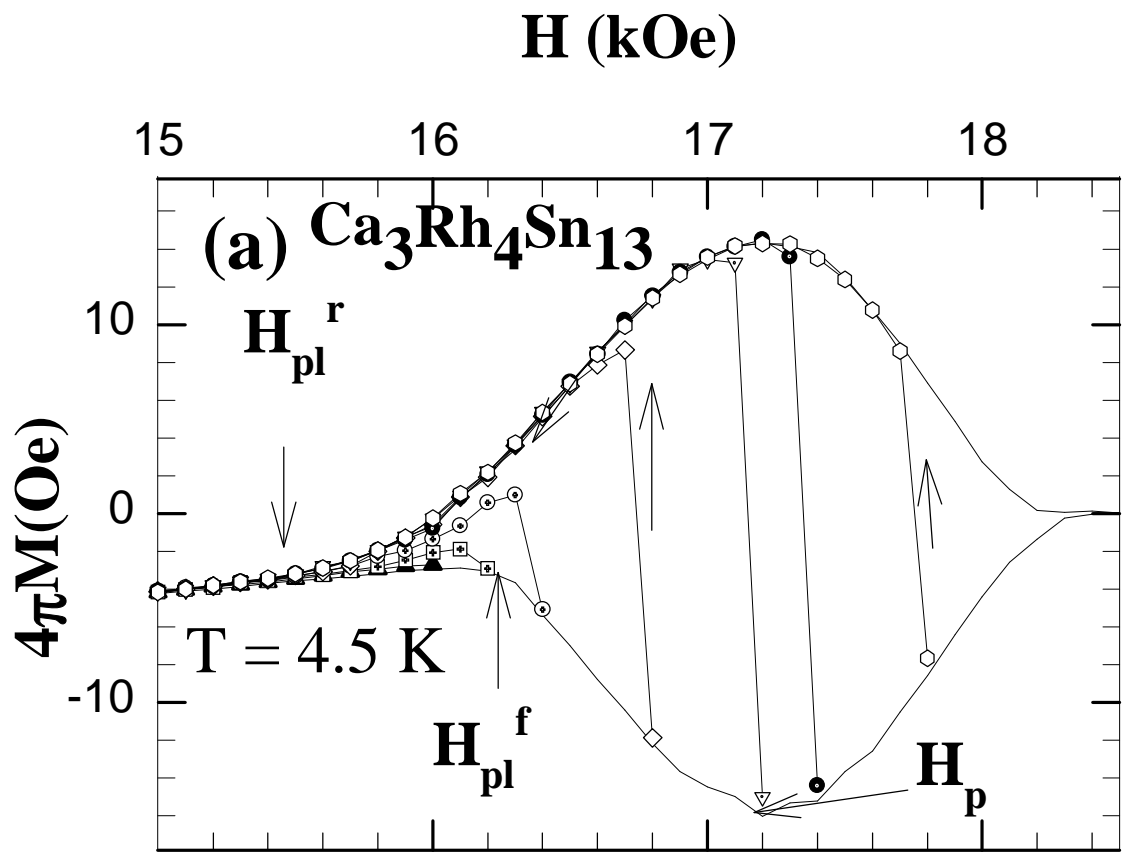


Fig. 7 Sarkar et. al.

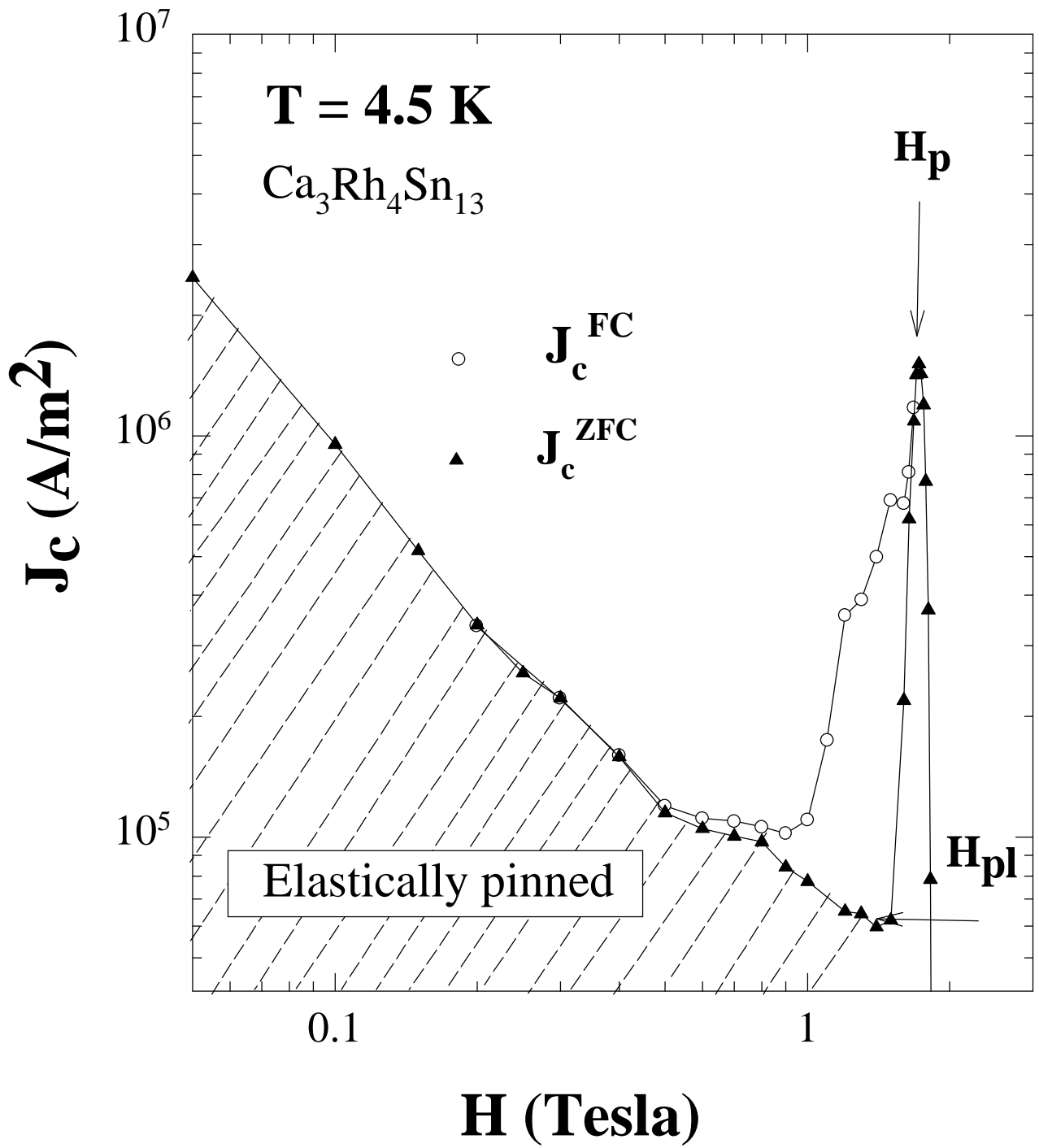


Fig. 8 Sarkar et al

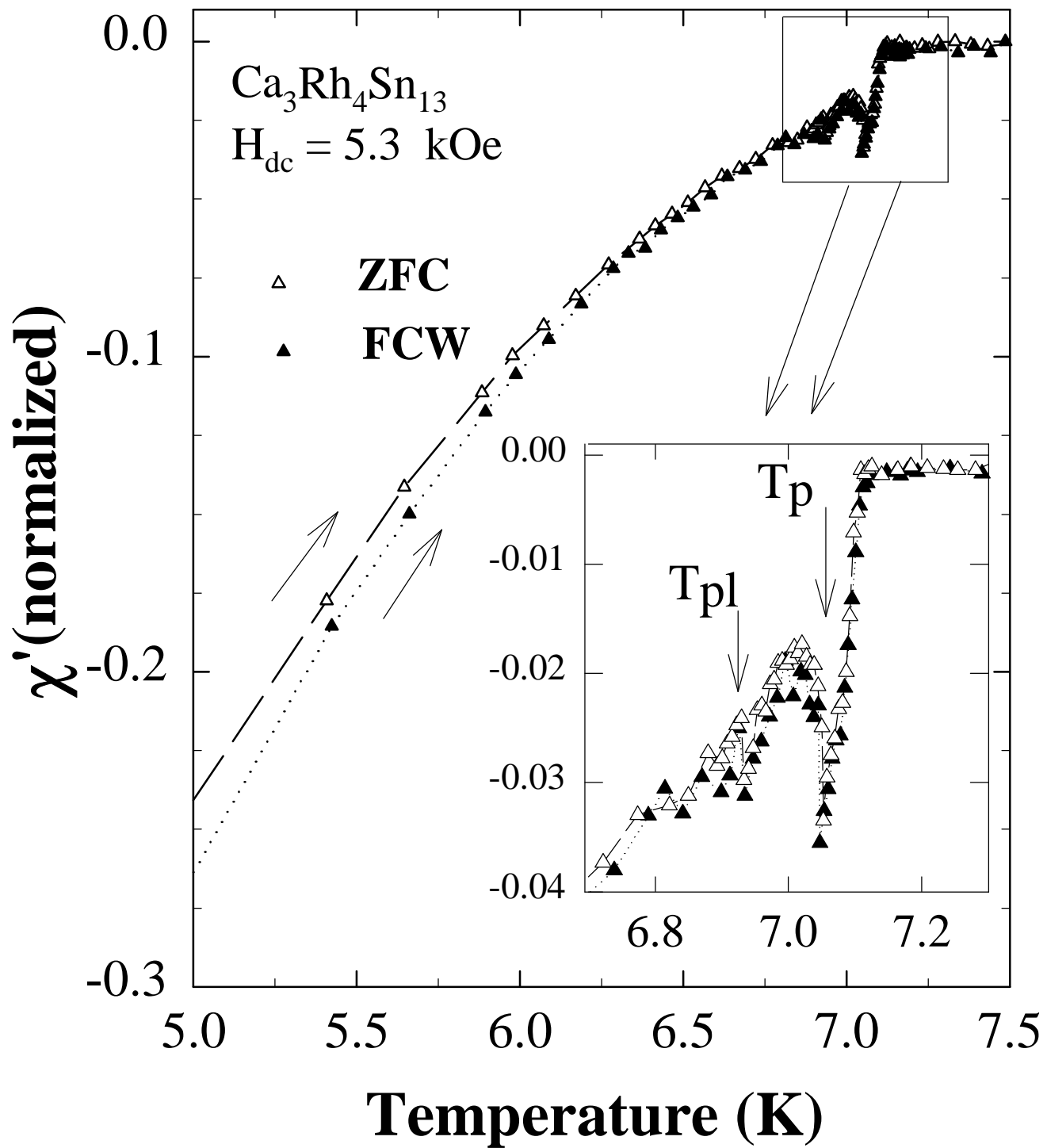


Fig. 9 Sarkar et al

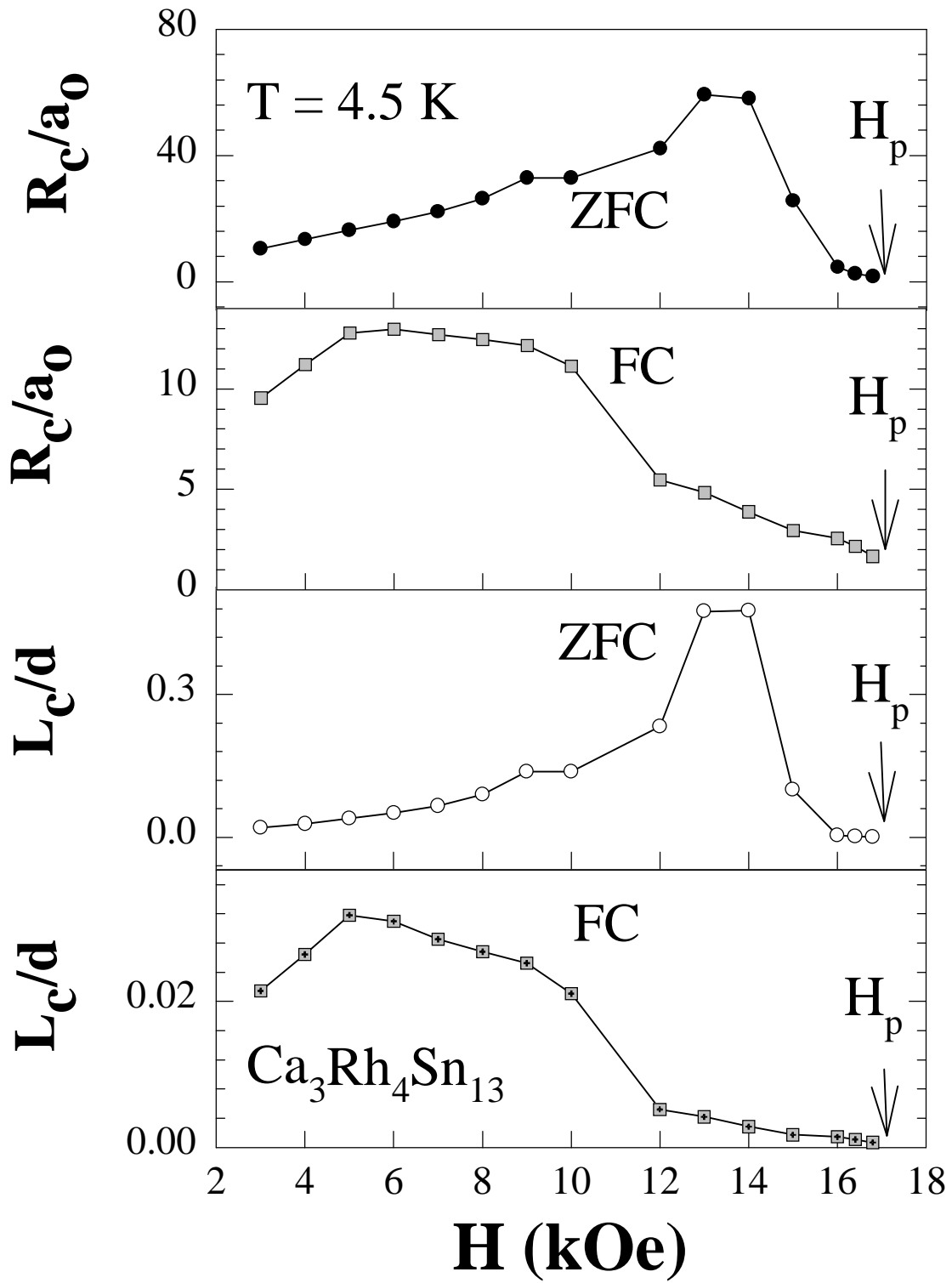


Fig. 10 Sarkar et al

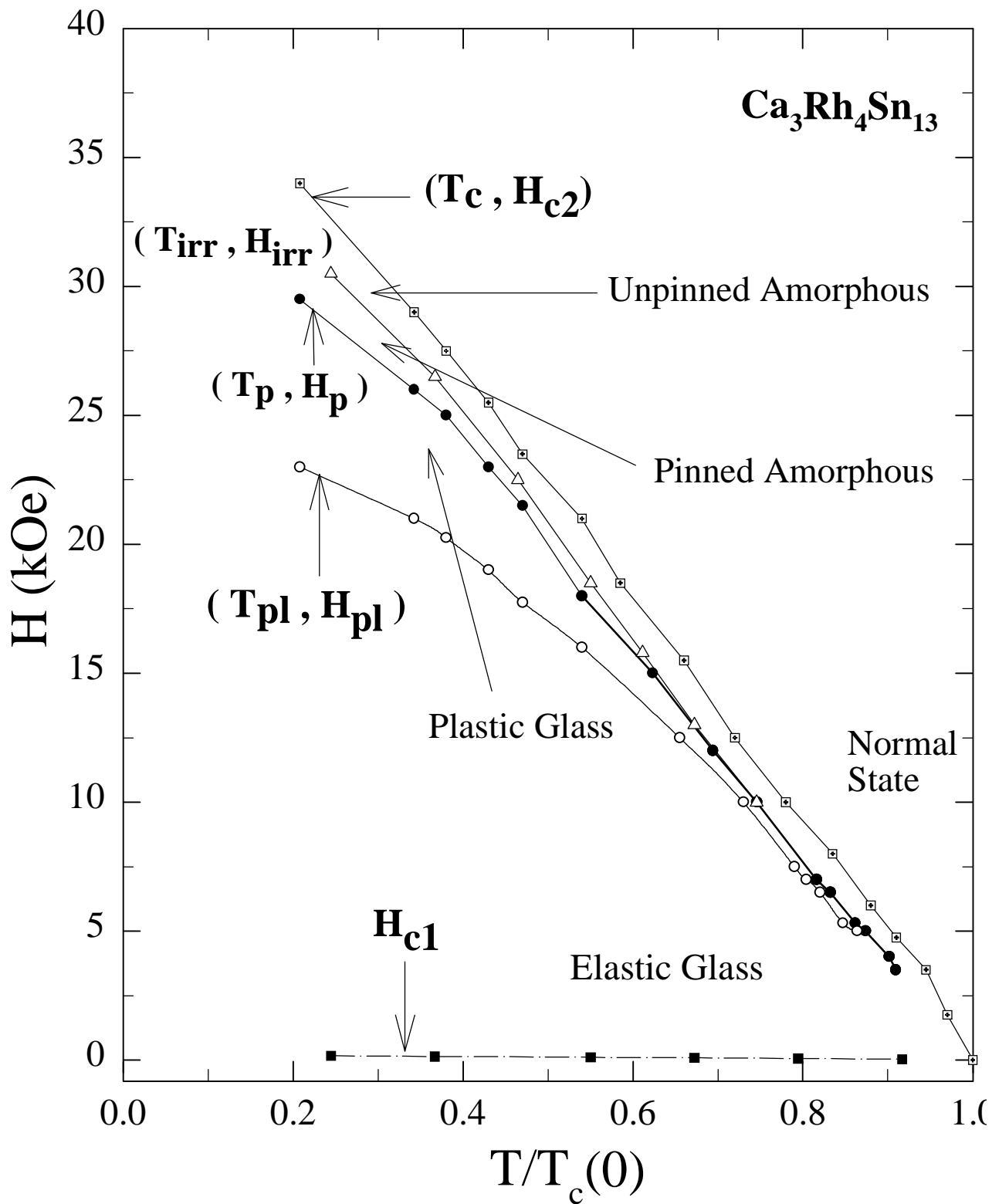


Fig. 11 Sarkar et al